ABSTRACT

RICK BOND: An Analysis of Density Enhanced Remediation of DNAPLs
(under the direction of Dr. Cass T. Miller)

The contamination of groundwater by dense non-aqueous phase liquids (DNAPLs) poses one of the most pervasive and difficult groundwater remediation problems in the field of environmental engineering. A new concept, density enhanced remediation of DNAPL (DERD), has been proposed by Dr. Cass T. Miller that relies upon mobilization of a DNAPL while controlling its vertical migration.

This report presents a conceptual model for the implementation of DERD and an analysis of the effects of selected decision variables on DERD process efficiency. Computer simulations were performed that modeled 1) injection of a dense brine into the subsurface to form a barrier against vertical DNAPL migration, and 2) subsequent extraction of the injected brine through production well(s). Dimensionless parameters formed from decision variables and hydrogeological characteristics were used to analyze simulation results, and an objective function, based on capital and recovery costs for the brine, was calculated for each simulation to rank decision variable strategies. The computer code used for this study (HST3D, developed by the U. S. Geological Survey) employs finite difference methods to solve three-dimensional groundwater flow, heat, and solute transport in a saturated porous medium.

Analysis of the results revealed an optimal range of production and injection rates for each specified well spacing configuration that minimized the unit cost objective function. In addition, the objective function was minimized by injection to production rate ratios near 1.0 and by use of variable pumping rates for both the injection and production wells. Brine recovery efficiency was improved by extraction through multiple wells rather than the central well alone.

High permeability and low permeability homogeneous medium simulations resulted in similar unit costs and quantities of brine, but the time scales required to complete the process were significantly longer for low permeability soil. Segmentation of the simulation domain into strata with different soil permeability resulted in less efficient brine injection and higher brine unit costs.

ACKNOWLEDGEMENTS

I would like to take this opportunity to express my appreciation for the tremendous help and support I received preparing this report. I would like to thank Dr. Miller for allowing me to work on this project and for broadening my engineering horizons with an introduction to groundwater engineering. My academic advisor, Dr. DiGiano, has been a constant source of support and inspiration. Of the dozens of times I knocked on his door during the last year and a half, Dr. DiGiano, without fail, made time to answer my questions or offer advice. My officemate, Joe Kanney, was a tremendous source of help with technical questions about modeling, the UNIX operating system, groundwater, and too many other subjects to list here. I want to thank Dr. Brubaker for taking time out of his busy schedule to be on my committee. Finally I would like to thank my wife, Donna Jennings, for her love, support, and understanding throughout the pursuit of my Masters degree.

TABLE OF CONTENTS

LIST OF FIGURES

LIST OF TABLES

1 INTRODUCTION

The contamination of groundwater by dense non-aqueous phase liquids (DNAPLs) poses one of the most pervasive and difficult remediation problems in the field of groundwater engineering (7, 10, 20). DNAPLs are volatile organic chemicals characterized by immiscibility with water and specific gravities greater than one (7,12). DNAPLs commonly encountered in contaminated groundwater include chlorinated solvents such as carbon tetrachloride, dichlorobenzenes, trichloroethylene (TCE), tetrachloroethylene (PCE), trichloroethanes, and dichloroethanes (7). All of the above are regulated by EPA under the Safe Drinking Water Act at minimum contaminant levels (MCLs) ranging from 0.002 to 0.2 mg/L, and all but trichloroethane are classified by EPA as probable human carcinogens (22).

DNAPLs have widespread industrial application and are commonly found in dry cleaning agents, grain fumigants, solvents, refrigerants, metal degreasers, paint and varnish removers, and in the manufacture of vinyl chloride (7). Wide-ranging industrial use of DNAPLs combined with instances of poor handling and disposal practices, particularly in the 1960s and 1970s, have resulted in extensive DNAPL groundwater contamination in the United States and other industrialized countries. The difficulty inherent in remediating DNAPL contaminated sites and the pervasiveness of this contamination is evidenced by the volume of research and the variety of remediation methods applied to the problem in the last twenty years.

In the subsurface, DNAPL can exist as a free phase, solubilize into water, sorb to the solid phase, or volatilize to the gas phase (7). The difficulty in removing a DNAPL from subsurface environments derives primarily from its limited solubility in water and its density (7, 12, 17, 19, 20, 25). Table 1.1 lists some typical DNAPL densities and solubilities (7, 12).

Table 1.1 – Characteristics of Typical DNAPLs

DNAPL	Density (g/cc)	Solubility Limit (mg/L)	Boiling Point at 760 mm (°C)
Carbon Tetrachloride	1.59	785	75.6
1,1-Dichloroethane	1.17	5500	57.3
Trichloroethylene (TCE)	1.46	1100	88.0
1,1,1-Trichloroethane	1.35	480-4400	74.1
1,1-Dichloroethylene	1.22	400	31.7
Tetrachloroethylene	1.63	150-200	121.2

A DNAPL released into the subsurface is subject to gravity forces, viscous forces due to groundwater flow, and capillary forces due to interfacial tension between the DNAPL and water (1, 7, 19, 20, 25, 26). Since it is denser than water, a DNAPL migrates vertically until capillary forces are great enough to counteract gravity and viscous forces. When this state of equilibrium is reached, DNAPL becomes entrapped in the porous medium, in either single or multiple connected pore volumes (7, 19, 20, 25, 26).

Entrapped DNAPL, or DNAPL residual, creates a three-fluid-phase system with gas and water in the unsaturated zone and a two-fluid-phase system below the water table (7, 20, 25). Since water typically is the wetting phase in a DNAPL-water system, DNAPL fills the larger pore volumes below the water table, resulting in pools of DNAPL locked in place until either capillary forces are overcome or interfacial tensions are reduced (7,20,23). Because residual DNAPL is immobile, mass transfer assumes primary importance, either directly or indirectly, as a removal mechanism.

Ironically, mass transfer itself is retarded by the presence of the trapped DNAPL pools. In a multiphase system, the hydraulic conductivity of the wetting phase in a porous media is reduced proportionately by the presence of a nonwetting phase (1, 7). This hindrance of flow through the contaminated region limits mass transfer to the regions through which water flows.

In the past twenty years, DNAPL remediation strategies have included pump-and-treat, vapor extraction, in-situ biodegradation, and steam injection (2,7,8,9,10,24) . All of these methods rely either directly or indirectly on mass transfer.

Recently more aggressive remediation methods, often grouped under the term "enhanced remediation", have achieved success using injections of chemical solutions to increase the solubility and decrease the interfacial tensions of nonaqueous phase liquids (NAPLs) (4,15,17,18,24,25,27) . The two major enhanced remediation methods being researched and implemented today are cosolvent flushing (CF) and surfactant flushing (SF).

The reduction in interfacial tensions and the resulting potential for DNAPL to be mobilized and migrate vertically into previously uncontaminated regions has led many researchers to recommend that surfactants and or cosolvents not be used for DNAPL remediation (4, 5). Other researchers, such as Sabatini et al, 1999, have focused on the development of surfactants that do not result in DNAPL mobilization, even though research indicates that removal efficiency is much greater when mobilization occurs (25).

A new concept, density enhanced remediation of DNAPL (DERD), has been proposed that relies upon mobilization while providing a protective barrier against contaminant spread (19,20). The goal of this concept, to maximize DNAPL removal efficiency while providing a physical barrier to DNAPL migration, implies that DERD is a potentially promising DNAPL remediation strategy.

In DERD, a density or capillary barrier consisting of a salt solution denser than the subject DNAPL is established below the contamination region. This density barrier serves the following two functions:

1. DNAPL pools lying atop soil strata of relative low permeability are lifted by buoyant forces and supported at the top of the density barrier where the free DNAPL may be withdrawn with a production well.

2. Vertical migration of mobilized DNAPL is stopped at the density barrier, preventing further vertical migration of DNAPL, as a separate phase. The free phase and solubilized DNAPL collected at the surface of the density barrier are accessible for production well extraction.

The objectives of this report are as follows:

1. to present a conceptual model for the implementation of DERD; and

2. to evaluate the effects of selected decision variables on DERD process efficiency.

2 BACKGROUND

Pump-and-treat (PAT) historically has been the most widely used method in groundwater remediation but has proven to be singularly inefficient in removing DNAPL (4,5,7,12,19,20,25). PAT relies on well-induced groundwater flow through the contaminated region to remove a dissolved contaminant, which is then removed from the groundwater in above ground treatment processes.

DNAPL, however, is only slightly soluble in water (5,7,12,25), and mass transfer is further hampered by the reduction in hydraulic conductivity caused by DNAPL pools and the consequent flow of water around rather than through regions of high DNAPL concentration (1,7). Therefore PAT efficiency is severely limited by DNAPL mass transfer rates, and DNAPL remediation often requires very long time scales and many pore volumes of pumped water to effect any significant reduction in a DNAPL source. In many cases, PAT has only been effective in containing the dissolved DNAPL plume, and once pumping is stopped, the plume is reestablished from the DNAPL source (12).

Vapor extraction (VE) also uses wells to induce flow and mass transfer of a contaminant, but in VE, wells are used to draw a vacuum in the unsaturated zone and create a pressure gradient resulting in convective gas flow up through the vandose zone. DNAPL is volatilized to the gas phase and the off gas is collected at the surface for treatment (7,9). This strategy can be effective for removal of residual DNAPL in the unsaturated zone since many DNAPLs are relatively volatile, but VE is not effective in removing DNAPL in the saturated zone (7, 20). The interface for DNAPL mass transfer from the saturated zone to the gas phase occurs only at the water table surface. Since DNAPL is denser than water, most of the DNAPL volume will reside below the water table surface unavailable for mass transfer to the gas phase.

DNAPL remediation via in situ biodegradation occurs naturally and can be engineered with the introduction of suitable microbes to contaminated regions (7,24).

Many DNAPLs are toxic to degradative bacteria; therefore bioremediation can only successfully occur after the free DNAPL has been solubilized. In addition, some DNAPLs have limited biodegradability (7), and further reductions in biodegradation rates occur when a suitable electron acceptor is not present in sufficient concentration. The biodegradation rate can also be limited by DNAPL-to-water mass transfer since only DNAPL in solution with water is available to the microbes as substrate.

In the steam injection (SI) process, steam is injected into the subsurface to heat DNAPL to its boiling point and subsequently remove it via volatilization (7,12). The major drawbacks to SI are the energy requirements to heat not only the DNAPL but also the surrounding water and soil, and the potential for DNAPL migration into uncontaminated regions (7,20). When DNAPL is heated a variety of physicochemical changes occur, including reduction in surface tensions, resulting in the potential for DNAPL mobilization and migration into uncontaminated regions (12,20).

Cosolvent flushing and surfactant flushing both employ a chemically enhanced PAT strategy, and the two differ essentially only in the type of chemical injected (4,5,7,17,25). In CF an alcohol-water mixture is injected into the subsurface, and in SF a surfactant is injected. In CF and SF, a contaminated region is rinsed with a chemical solution delivered through strategically spaced injection wells with the goal of increasing DNAPL solubility. The withdrawal and treatment of groundwater then is identical to PAT except that groundwater is withdrawn at much higher DNAPL concentrations than are achievable in a water solution, thereby significantly reducing the time required for remediation. The efficiency of enhanced methods is often measured in pore volumes (PV) of chemical injected to achieve a percentage of DNAPL removal (17,19).

An essential difference in the behavior of surfactants and alcohols is the ability of surfactants to self-aggregate into micelles once the surfactant surpasses a critical micelle concentration (CMC) (25). Micelle formation increases the effective solubility of DNAPL by capturing DNAPL in the hydrophobic interior of a micelle whose hydrophilic exterior is highly soluble in water.

The degree to which a surfactant partitions to either the water or the DNAPL phase depends on its hydrophilic-lipophilic balance (HLB). Surfactant HLB values range from 5 to 20, with hydrophilic surfactants at the high end of the scale and lipophilic surfactants at the low end (25). The transition from hydrophilic to lipophilic surfactant begins at HLB values of about 10 to 12 (25), and surfactants in this range can form "middle phase microemulsions". Middle phase microemulsions, liking neither oil nor water, accumulate as a separate thermodynamically stable phase at the DNAPL-water interface. Development of middle phase microemulsions is significant in DNAPL remediation because solubilization potential is maximized and interfacial tensions are minimized in this narrow HLB range, thereby optimizing DNAPL removal (25).

Researchers have found DNAPL solubilities to be typically almost 100,000 times greater in surfactant enhanced systems than in water alone (4,5,7,17,18,20,25,27), and field tests have been performed in which 86% of an original 55,000 mg/kg dry soil DNAPL concentration has been recovered after only a 0.9 pore volume sweep of surfactant (17).

Microemulsions dramatically reduce DNAPL-water interfacial tensions causing free DNAPL to be mobilized. Sabatini et al. (1999) demonstrated that mobilization of DNAPL begins at interfacial tensions slightly less than 4 dynes/cm. In batch tests of surfactants, researchers have found DNAPL-water interfacial tensions as low as 0.005 dynes/cm, and values in hundredths of dynes/cm are typical (25). The ultra-low interfacial tensions developed in surfactant systems portend significant mobilization of free DNAPL, and in fact researchers have documented that mobilization far outperforms solubilization in surfactant-enhanced extraction of DNAPL (25).

Heretofore the potential for DNAPL mobilization and vertical migration has been considered a serious disadvantage in the use of enhanced remediation for DNAPL extraction. Researchers either have recommended that surfactants and or cosolvents not be used for DNAPL remediation (5) or have concentrated efforts on finding surfactant solutions that maximize solubilization while maintaining interfacial tensions above the DNAPL mobilization threshold (25,27).

The first approach discards one of the most promising strategies for DNAPL remediation as posing too great a risk for contamination spread. The second approach limits the types of surfactants that can be used to those that do not risk DNAPL mobilization. While this method has been successfully implemented in lab and field tests (25), the strategy

1. fails to completely maximize solubilization potential;
2. does not take advantage of the greater removal efficiencies afforded by mobilization;
3. limits one's capacity to select a surfactant based on optimization of performance and cost factors; and
4. risks spreading the contamination if the surfactant is not chosen carefully for its impact on interfacial tensions.

DERD appears to have the potential to address these liabilities and provide dramatic increases in DNAPL remediation efficiency. DERD implementation currently is being tested in the laboratory (19), and this paper describes the first attempt to model DERD with computer simulations.

In the ongoing lab work, one-dimensional column tests and two-dimensional flow cell tests have been performed using a packed heterogeneous media contaminated with TCE (19). Tests were performed with a two fluid system using water for the flushing fluid and a NaI solution for the density barrier and a three fluid system that in addition to water and a NaI solution, employed a surfactant as the flushing fluid.

In the two fluid system, 54% to 74% of the TCE was removed with less than a one pore volume sweep of water. In the three fluid test, over 90% of the TCE was removed with less than a one pore volume sweep of surfactant. The brine density barrier was successful both in floating DNAPL from the bottom of the medium and in completely stopping the vertical migration of DNAPL.

The first attempt at using computer modeling to simulate field applications of DERD is the subject of this report. Computer modeling has been a valuable and economical tool in the analysis and prediction of subsurface groundwater system behavior. The surge in recent years in computing power and speed has led to increased activity in the development and use of modeling programs that employ numerical methods to solve large and complex groundwater problems (6,13).

3 METHODS

In a typical implementation of DERD, a set of strategically located production and injection wells operate in concert to treat a contaminated area. The DERD implementation modeled for this report consists of a central production well surrounded by four uniformly spaced injection wells, which in turn are bounded by an outer perimeter of four production wells.

The well group described above acts as a unit to 1) develop a density barrier below the contaminated region, 2) draw the water table down preparatory to surfactant flushing, and 3) to remove the DNAPL, surfactant, and brine. The design values selected for injection and production well perimeters, total well production and injection rates, and the ratio of total injection to production rates effect the efficiency of DERD.

In the first stage of DERD, the brine density barrier must be established prior to mobilization of DNAPL. Brine injection is initiated with simultaneous production well withdrawal in a ratio designed to cause the water table to be lowered concurrent or shortly after the complete establishment of the brine density barrier. DNAPL pools that have collected on the surface of relatively impermeable soil stratum are floated to the surface of the density barrier by buoyant forces, and some DNAPL mobilization begins with the dewatering process.

Once the density barrier and desired drawdown of the water table are established, surfactant is injected into the contaminated region, and mobilized free phase DNAPL and DNAPL saturated groundwater flow downward and toward the production wells. The density barrier stops the vertical migration of DNAPL, and DNAPL is extracted through production wells. Once the DNAPL has been extracted, the injection wells are turned off, and the brine is recovered in the production well(s) for treatment and recycle.

The advantages of this system include the following:

- DERD provides a physical barrier against DNAPL migration to uncontaminated regions.

- DERD utilizes DNAPL mobilization, which has been shown to result in much higher extraction efficiencies than solubilization alone (25). Greater extraction efficiencies can result in less surfactant and less time required to achieve cleanup goals.

- Surfactant selection is not limited to surfactants that maintain interfacial tensions above the mobilization threshold. Removing this constraint to cost minimization could result in the selection of a less expensive surfactant relative to the CF process.

- In addition to DNAPL, surfactant is also captured by the density barrier resulting in greater surfactant recovery.

- If evaporation is used to recover brine, DNAPL removal could be a precursory result of the brine recycling process (see boiling point temperatures, Table 1.1).

3.1 Objective Function

Costs associated with the brine are both the dominant and most variable factors in the total cost of the density enhancement aspect of the process, therefore an objective function comprised of brine capital cost, recovery cost, and salvage value was used as the determinant of process efficiency. Brine capital cost was based on a manufacturer quote for $CaBr_2$ delivered to a site. Recovery cost was based on the energy cost to reconcentrate the brine via water evaporation, and this cost is a function of the brine concentration of groundwater as it is withdrawn from the soil. The closer the recovery brine concentration is to the required injection concentration, the less water must be evaporated to achieve recovery. Salvage value was estimated to be 80% of capital cost, based on a manufacturer quote.

The capital cost in the objective function is based on a manufacturer quote of $130 per 42 gallon barrel for $CaBr_2$ brine delivered to a site ($0.52 per kg) at a density of 1600 g/cc, the density at which the brine is injected in all of the simulations of this report.

The treatment unit cost is based on an estimated energy cost of $0.025 per pound of water removed by evaporation assuming electricity as the energy source. This cost was provided by Tetra Technologies and is confirmed in the calculation in Table 3.1. The constants used in the calculation of energy costs are listed in Table 3.2.

Table 3.1 – Energy Cost for Evaporative Brine Recovery

Initial Water temperature °C	Energy to heat water to 100 °C (kJ /kg)	Energy for vaporization (kJ /kg)	Total Energy (kJ /kg)	Total Energy (kWh/kg)	Cost Electric ($/kg)	Cost Electric ($/lb)	Cost Gas ($/kg)	Cost Gas ($/lb)
15	355.3	2260	2615.3	0.73	0.06	0.026	0.019	0.008
20	334.4	2260	2594.4	0.72	0.06	0.025	0.018	0.008
25	313.5	2260	2573.5	0.71	0.06	0.025	0.018	0.008

Table 3.2 – Constants Used in Table 3.1 Energy Cost Calculations

Water Specific Heat	4.18kJ/kg-°C
Water Heat of Vaporization	2260kJ/kg
Electric Cost	0.07$ per kWh
Gas Cost	0.75$ per Therm (1 Therm = 105,500 kJ)
Efficiency	0.9

The cost for natural gas powered evaporation, also calculated in Table 3.1, is estimated to be approximately one-third the estimated cost for electricity. The analysis

throughout this report, however, is based on use of electricity since natural gas may not be available in all locations. The choice of energy unit cost does not effect the relative ranking of the strategies analyzed, only the magnitude of the costs calculated.

Table 3.3 illustrates the calculation of treatment unit costs, based on electrical energy costs, for brine recovered at various mass fractions, and Figure 3.1 depicts the relationship graphically. The cost to concentrate the brine and the unit cost for brine recovery were calculated in Table 3.3 according to the following algorithm:

$$Mw = 1 - w$$

$$Mwr = Mw - w$$

$$Mb = 2w$$

$$C = 0.06\ Mwr$$

$$Cb = C / Mb = 0.06\ (0.5/w - 1)$$

Where

w = solute mass fraction (kg solute / kg solution)

Mw = mass of water in one kg solution with mass fraction w (kg)

Mwr = mass of water that must be removed from one kg solution of mass fraction w (kg)

Mb = mass of brine recovered at a mass fraction of 0.50 (kg)

C = cost to recover Mb ($)

Cb = unit cost to recover Mb ($ per kg brine recovered)

Table 3.3 – Calculation of Brine Recovery Unit Costs

Mass fraction	Mass of water per kg total mass	Mass of solute per kg total mass	Mass of water removed per kg total mass	Mass of brine solution recovered per kg total mass	Cost to recover brine solution	Unit Cost per kg solute recovered
w (kg/kg)	Mw (kg)	Ms (kg)	Mwr (kg)	Mb (kg)	C	Cb
0.01	0.99	0.01	0.98	0.02	$ 0.054	$ 2.71
0.02	0.98	0.02	0.96	0.04	$ 0.053	$ 1.33
0.03	0.97	0.03	0.94	0.06	$ 0.052	$ 0.87
0.04	0.96	0.04	0.92	0.08	$ 0.051	$ 0.64
0.05	0.95	0.05	0.9	0.1	$ 0.050	$ 0.50
0.06	0.94	0.06	0.88	0.12	$ 0.049	$ 0.41
0.07	0.93	0.07	0.86	0.14	$ 0.048	$ 0.34
0.08	0.92	0.08	0.84	0.16	$ 0.046	$ 0.29
0.09	0.91	0.09	0.82	0.18	$ 0.045	$ 0.25
0.1	0.9	0.1	0.8	0.2	$ 0.044	$ 0.22
0.2	0.8	0.2	0.6	0.4	$ 0.033	$ 0.08
0.3	0.7	0.3	0.4	0.6	$ 0.022	$ 0.04
0.4	0.6	0.4	0.2	0.8	$ 0.011	$ 0.01
0.5	0.5	0.5	0	1	$ -	$ -

Figure 3.1 – Brine Recovery Unit Cost vs. Recovery Mass Fraction

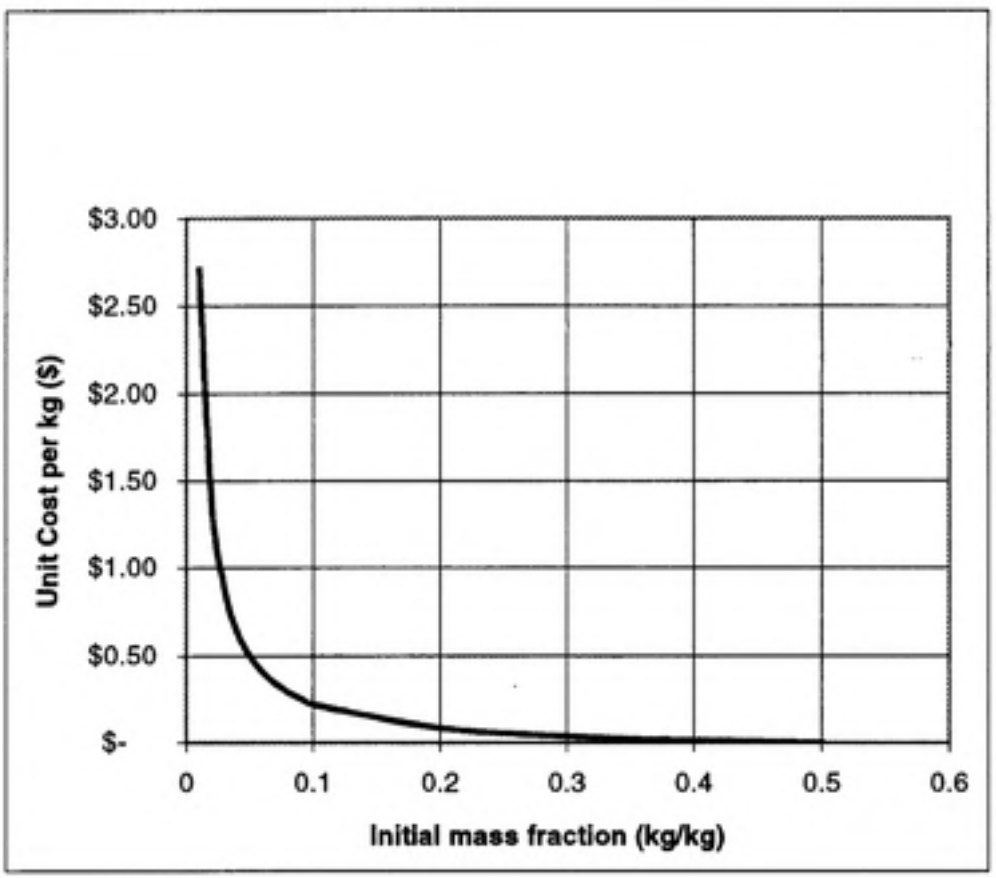

In Figure 3.1, it is clear that the unit cost for brine recovery begins to increase sharply with decreasing mass fraction below 0.10 kg/kg. In a comparison of capital cost to recovery cost for brine, the calculations in Table 3.3 indicate that it becomes less expensive to purchase new brine than to recover brine at mass fractions less than 0.04 when electricity is the power source.

In this report, the cost objective function is used as a tool to comparatively rank the efficiency of different implementation strategies rather than as an evaluation of cost feasibility. Since the decision to use DERD can affect many other cost variables, e.g. the type of surfactant that can be used, the amount of surfactant required, time required for cleanup, a true cost feasibility analysis should be based on site-specific application of all cost variables.

Recovery of brine below a mass fraction of 0.04 is not cost effective. Consequently simulations were ended when the recovered brine mass fraction reached 0.04 or a concentration of 40,000 mg/L at the recovery well. Regardless of the ratio of capital to recovery costs, however, federal and local environmental regulatory agencies will require that a specified minimum percentage of the brine be removed from the site. In practice, current applicable regulations will add a constraint in optimizing the cost function, and if allowable, discharge of recovered brackish groundwater to surface waters or municipal sanitary sewers may be less expensive than recovery at low mass fractions.

It is highly likely that continued development of DERD would lead to the discovery of less expensive brines and recovery processes. Reverse osmosis, for example, may hold promise for pre-concentrating brines recovered at low mass fractions prior to evaporation (10). Generally, however, treatment process costs are proportional to the difference between influent and effluent concentrations, therefore a change in treatment process may affect the total cost estimated for a simulation but not the efficiency of one simulation relative to another.

3.2 Model Description

In this analysis, computer simulations were used to develop a conceptual model for implementation of DERD and to evaluate the effects of various decision variables on process efficiency.

There are a handful of programs that model density dependent flow, and considerable modeling efforts have been applied to this topic, particularly in the area of

saltwater encroachment (6,13). The program used in this analysis, HST3D, was first developed in 1985 at the United States Geological Survey (USGS), and the version used for this analysis, V 5.01, was released in 1998 (14).

HST3D uses finite difference methods to solve three dimensional groundwater flow, heat, and solute transport in a saturated porous medium by solving:

1. saturated groundwater flow using conservation of fluid mass and Darcy's equation for flow in a porous media;

2. heat transport from the conservation of enthalpy; and

3. transport of solute from the conservation of mass for a single solute fluid.

Groundwater flow and solute transport are coupled through the dependence of advective and dispersive transport on interstitial fluid velocities, the dependence of fluid viscosity on solute mass fraction and temperature, and the dependence of density on solute mass fraction, temperature, and pressure. Heat transport was assumed to be insignificant in this application, and fluid compressibility was assumed to be zero. Consequently, fluid viscosity and density were reduced to functions solely of solute mass fraction.

Pressure is the dependent variable in the flow equation (14), and the equation as shown below is derived from the conservation of fluid mass coupled with Darcy's equation for flow through a porous medium.

$$\frac{\partial(\varepsilon\rho)}{\partial t} = \nabla \cdot [\rho \mathbf{K} \cdot \nabla \phi] + q\rho^*$$

where

ρ = fluid density (kg/m^3)

ε = effective porosity

t = time (s)

K = fluid hydraulic conductivity (m/s)

ϕ = piezometric head (pressure head plus elevation head) (ft)

ρ^* = density of fluid source/sink (kg/m^3)

q = fluid source/sink specific discharge (m^3/m^2 - s)

The transport equation expresses conservation of mass with mass fraction the dependent variable (14).

$$\frac{\partial}{\partial t}(\varepsilon + \rho_b K_d)\rho\ w = \nabla \cdot [\rho\, \varepsilon\, (\mathbf{Ds} + \mathrm{Dm}\ \mathbf{I})\nabla w] - \nabla \cdot [\varepsilon\, \rho\, \mathbf{v}w] - \lambda\, (\varepsilon + \rho_b K_d)\rho\, w + q\rho^* w^*$$

where

w = mass fraction

w * = fluid source/sink mass fraction

Ds = mechanical dispersion coefficient tensor (m^2 /s)

Dm = effective molecular diffusivity of the solute (m^2/s)

λ = linear decay constant (s^{-1})

K_d = distribution coefficient (m^3 / kg)

ρ_b = bulk density of porous medium (kg/m^3)

I = identity matrix of rank 3

v = interstitual velocity vector (m/s)

For a conservative salt undergoing neither sorption nor chemical reaction, the third term on the right side of the equation drops out.

HST3D assumes fluid density to be a linear function of pressure, temperature, and solute mass fraction.

$$\rho\,(p, T, w) = \rho_0 + \rho_0 \beta_p\,(p - p_0) - \rho_0\, \beta_T\,(T - T_0) + \rho_0 \beta_w\,(w - w_0)$$

where

T = fluid and porous medium temperature (°C)

T_0 = reference fluid and porous medium temperature (°C)

p = fluid pressure (Pa)
p_0 = reference fluid pressure (Pa)
w = fluid mass fraction (kg solute/kg fluid)
w0 = reference fluid mass fraction (kg solute / kg fluid)

β_p = fluid compressibilty (Pa^{-1})
β_T = fluid coefficient of thermal expansion ($°C^{-1}$)
β_w = slope of fluid density as a function of mass fraction divided by reference fluid density
ρ_0 = fluid density at reference conditions (kg/m^3)

The fluid compressibility and temperature effects are assumed to be negligible thereby reducing the second and third terms in the above equation to zero and leaving density as a linear function of mass fraction.

HST3D employs a fluid-viscosity function in which viscosity is a function of temperature and mass fraction ignoring pressure effects. The equation allows a maximum mass fraction of 0.25, the solubility limit of NaCl. Given that densities greater than that attainable at a maximum mass fraction of 0.25 are required and temperature plays no part in the simulations, a new fluid-viscosity function was written into the code. The new fluid-viscosity function was based on empirical data for NaI as illustrated in Table 3.4 (16). Figure 3.2 shows the data represented graphically with a least squares fit equation plotted on the data.

Table 3.4 – NaI Density-Viscosity Data at 25° C

molality m	solute wt (g)	solvent wt (g)	Total wt (g)	mass fraction	density (g/cc)	viscosity (pa-s)	density (g/cc)
0	0	1000	1000	0.00	0.997	0.00089	
0.5	76	1000	1076	0.07		0.000904	1.054
1	153	1000	1153	0.13		0.000914	1.112
1.25	191	1000	1191	0.16		0.000921	1.114
1.5	229	1000	1229	0.19		0.000933	1.169
1.75	268	1000	1268	0.21		0.000945	1.197
2	306	1000	1306	0.23		0.000959	1.226
2.25	344	1000	1344	0.26		0.000973	1.255
2.507	383	1000	1383	0.28	1.258	0.000987	1.284
2.968	454	1000	1454	0.31	1.3	0.001023	1.337
5.107	781	1000	1781	0.44	1.48	0.001262	1.582
8.095	1238	1000	2238	0.55	1.689	0.001875	1.924
8.473	1296	1000	2296	0.56	1.712	0.00198	1.967

Figure 3.2 – NaI Density-Viscosity Relationship at 25° C

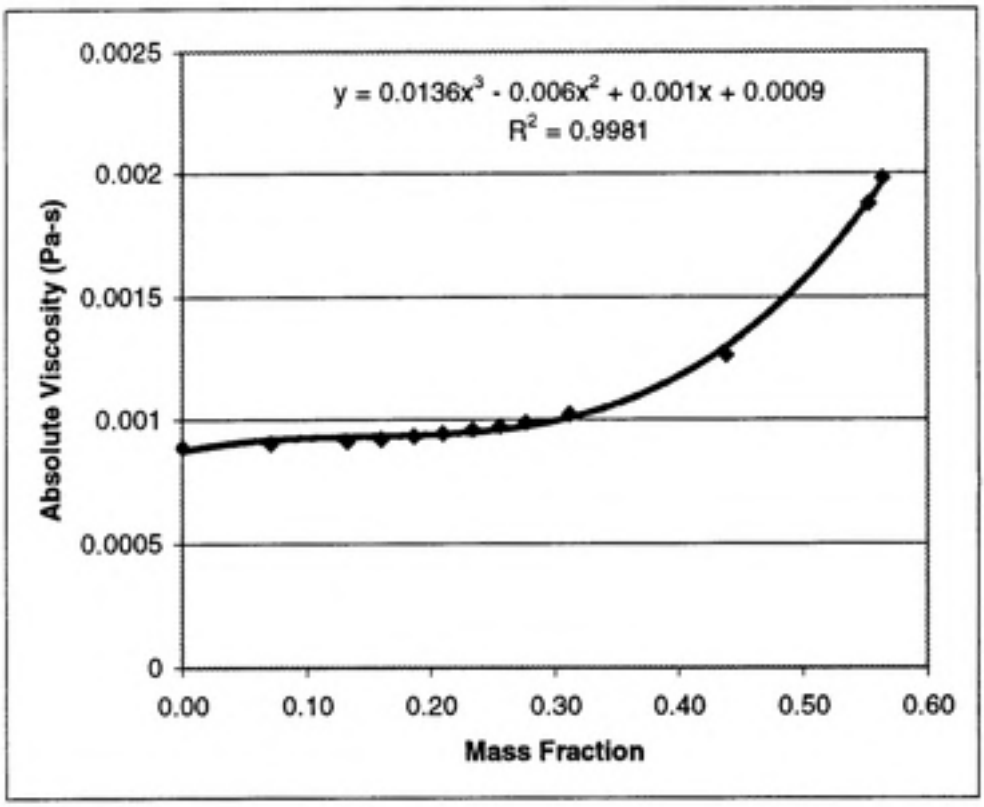

Mechanical Dispersion and molecular diffusion coefficients are combined into a single hydrodynamic dispersion coefficient tensor in HST3D.

$$D^*_{sij} = D_{sij} + D_m \delta_{ij}$$

where

D^*_{sij} = hydrodynamic - dispersion - coefficient tensor (m^2/s)

D_{sij} = mechanical dispersion tensor component (m^2/s)

δ_{ij} = Kronecker delta function

The medium was taken to be isotropic, and molecular diffusion effects were assumed to be negligible relative to mechanical dispersion. Therefore the components of dispersion coefficient tensor are described by longitudinal and transverse dispersivities.

$$D_{Sij} = (\alpha_L - \alpha_T)\frac{v_i v_j}{v} + \alpha_T v \delta_{ij}$$

where

α_L = longitudinal dispersivity (m)
α_T = transverse dispersivity (m)
v_i = component of velocity in i direction (m/s)
δ_{ij} = Kronecker delta function
v = magnitude of the velocity vector (m/s)

HST3D uses a modified version of the well-bore equation developed by Van Poolen and others (1968). The essence of this equation is the expression of well flow per unit length of well bore as a function of the pressure differential between the average pressure in the annulus between the well bore and the radius of influence. (See Kipp, 1987, for derivation of the well bore equations and a description of the options for well flow calculation).

HST3D uses finite differences method to approximate the partial differential equations (PDEs) presented above. A point-distributed grid is used for the spatial discretization. The grid is formed by specifying the distance between successive nodes in each coordinate direction. A cell volume is assigned to each node, formed by the cell planes or faces that bisect the distance between adjoining nodes.

A subdomain weighted-residual method is used in the spatial discretization with approximating functions that are piecewise linear for the dependent variables in the subdomain. The PDEs are discretized by integrating them over each cell volume. The Gauss divergence theorem is used to transform volume integrals of the divergence form into surface integrals, and the surface integrals are approximated by central or upstream differencing. For the integral of the time derivative, HST3D assumes the spatial average

over the cell volume can be approximated by the time derivative at each node. The flow and transport equations are solved sequentially with iteration for each time step until the convergence criteria are met or the maximum number of iterations is reached.

Identical initial and boundary conditions were used for all simulations. The initial conditions were hydrostatic pressure in an unconfined aquifer with a water table elevation of five meters and an initial mass fraction of 0.0 throughout the domain. First type or Dirichlet boundary conditions were specified with a constant potential of 5.0 meters at the four vertical boundary planes, a no flow boundary at the bottom plane, and a free surface condition at the top plane.

Dimensionless parameters developed from areas of well coverage, pumping rates, soil permeability, and hydraulic conductivity were the decision variables in the formulation of the DERD simulations.

3.3 Analysis

In practice, the geological, groundwater, and contaminant conditions will differ at each site, and each site should be evaluated as a unique problem. The intent of this analysis, however, was to identify general trends in DERD efficiency through dimensionless analysis.

Dimensionless parameters were formed from selected decision variables and media and fluid properties to allow inference of some general conclusions across the entire range of simulations regarding the effects of different decision variables on process efficiency. The dimensionless parameters are as defined in Table 3.5 below.

Table 3.5 – Dimensionless Parameters

Dimensionless Parameter	Definition
Q1'	Q2 / Q3
Q2'	Q1 / Q3
Q3'	Q3 / (A1 K_0)
A1'	k / A1
A2'	A1 / A2

where

Q1 = Well 1 production rate (m^3/h)

Q2 = total well injection rate (m^3/h)

Q3 = total production rate (m^3/h)

A1 = perimeter area of four injection wells (m^2)

A2 = perimeter area of four production wells (m^2)

k = soil permeability (m^2)

K_0 = hydraulic conductivity of water at 20° C

Simulations were conducted through a range of dimensionless parameter values to examine effects on DERD efficiency. The objective function was then applied to the results of each simulation as a means to quantify and rank comparative effectiveness of each simulation strategy.

Calculation of the objective function was performed by discretizing the cumulative mass recovery curve into representative time steps, then applying the cost function to each discrete time step mass using the average mass fraction between successive time steps. This calculation was performed individually for each well then

totaled for all wells and all time steps to derive the total brine recovery cost for the simulation. A brine capital cost was applied to the injected brine in each simulation at the unit cost to purchase new brine, and a salvage value of 80% of the purchase price was applied to the total mass of recovered brine. The total brine cost for each simulation was taken as the sum of the brine recovery and capital costs less the salvage value. This total cost was then normalized for the area treated to produce a brine unit cost per acre for each simulation. The unit cost per acre for brine was used as the objective function and the basis of comparison for simulations.

4 SIMULATIONS

A simulation domain 360 meters by 360 meters (horizontal plane) by 5 meters (vertical plane) was used for all simulations. The domain grid was uniform in the vertical plane with six nodes spaced one meter apart and symmetric in the horizontal plane. The horizontal plane grid spacing is shown in Table 4.1, and the vertical plane grid spacing in Table 4.2.

Table 4.1 – Domain Grid in the Horizontal Plane (X and Y coordinate directions)

X or Y Coordinate	Node Number	X or Y Coordinate	Node Number	X or Y Coordinate	Node Number
0	1	160	11	210	21
50	2	165	12	215	22
80	3	170	13	220	23
105	4	175	14	228	24
121	5	180	15	239	25
132	6	185	16	255	26
140	7	190	17	280	27
145	8	195	18	310	28
150	9	200	19	360	29
155	10	205	20		

Table 4.2 – Domain Grid in the Vertical Plane (Z coordinate direction)

Z Coordinate	Node Number
0	1
1	2
2	3
3	4
4	5
5	6

4.1 Initial and Boundary Conditions

The initial conditions were hydrostatic pressure in an unconfined aquifer with a water table elevation of five meters and a NaI initial mass fraction of 0.0 kg/kg fluid throughout the domain. First type, or Dirichlet, boundary conditions were specified with a constant potential of 5.0 meters at the four vertical boundary planes, a no flow boundary at the bottom plane, and a free surface condition at the top plane. Brine was injected at a mass fraction of 0.50 (1600 kg/m^3 density) with the goal of establishing a brine barrier beneath the contamination region with a minimum density of 1550 kg/m^3.

All of the simulations were performed with a transverse dispersivity of 0.05 m and a longitudinal dispersivity of 0.5 m, with the exception of one simulation performed with zero dispersivities to evaluate dispersion effects. All simulations assumed a medium porosity of 0.35 and zero medium bulk compressibility.

4.2 Well Configurations

All simulations were performed with nine wells, five production wells and four injection wells, located in the pattern illustrated in Figure 4.1. Well 1 in the center and Wells 6 through 9 forming the outer perimeter were the production wells. Wells 2 through 5 forming the inner perimeter were the injection wells. The wells were spaced uniformly in all simulations. Area "A1", formed by the injection well perimeter, and area "A2", the area included in the outer perimeter of production wells are denoted in Figure 4.1. All simulations were performed with a ratio of A2 to A1 of 4.0 (dimensionless parameter A2'). Variable "Q2" represents the total injection rate from Wells 2, 3, 4, and 5 and "Q3" the total production rate from Wells 1, 6, 7, 8, and 9.

The objective in terms of process efficiency (i.e. cost minimization) was to minimize the volume of brine required to treat a given area then to recover the brine at the highest concentration possible. The strategy behind the well configuration was to surround the injection wells with production wells to facilitate spreading of the brine, control the water table at the perimeter of the treatment region, and provide positive control against loss of brine beyond the system boundaries.

Figure 4.1 – Typical Well Configuration

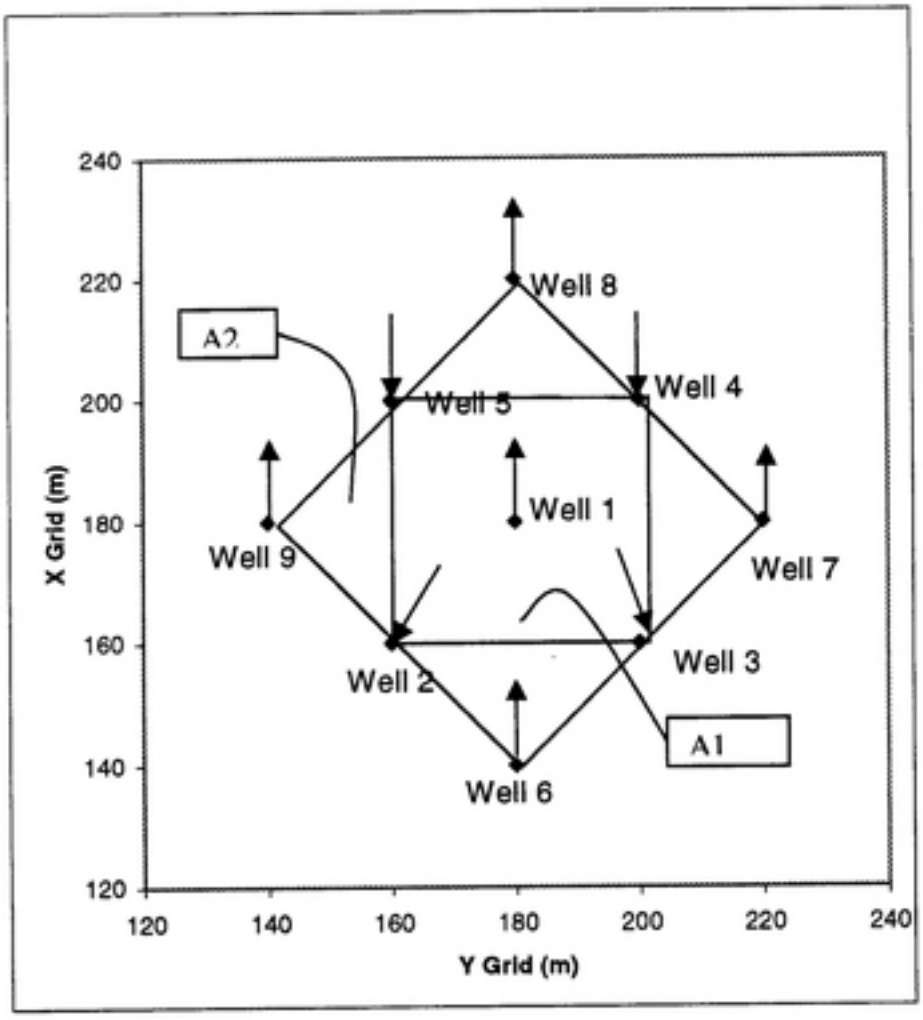

4.3 DERD Process Stage Description

The pumping process was performed in two stages. In the first stage, a ratio of total injection rate to total production rate (dimensionless parameter Q3') was established that allowed development of the density barrier and water table drawdown. Stage 1 was considered complete when a brine layer with a minimum density of 1550 kg/m^3 was established at the bottom of the contaminated region. (Though not modeled in these simulations, in a field application of DERD, contaminant would be withdrawn from the region above the brine layer during this stage). It should be noted that some subjective judgment was involved in the determination of density barrier establishment and the completion of Stage 1. Periodic assessments of simulation density profiles and solute mass balance were used to judge the point at which further injection would not yield increased density barrier coverage. Nonetheless, the corollary field decision is also necessarily reliant on engineering judgment and must be made with less data than is available in the simulated application.

In the second stage, brine was withdrawn from the domain until the mass fraction recovered in the well(s) fell to 0.04. In most simulations, recovery occurred through the center production well only, but recovery through the center well and the inner perimeter wells (with pumping direction reversed) was utilized in selected simulations for an efficiency comparison. The objective of the recovery process was to withdraw groundwater at the highest salt concentration possible to minimize brine recycle cost.

In Figure 4.2, recovery mass fraction at Well 1 is plotted against time for a typical simulation. (Typically half the solute mass was recovered through Well 1 with the remainder recovered either through Wells 6 to 9 during the injection stage or, in simulations in which Wells 2 to 5 were used for brine recovery, in Wells 2 to 9).

Figure 4.2 – Typical Solute Mass Recovery Diagram at Well 1

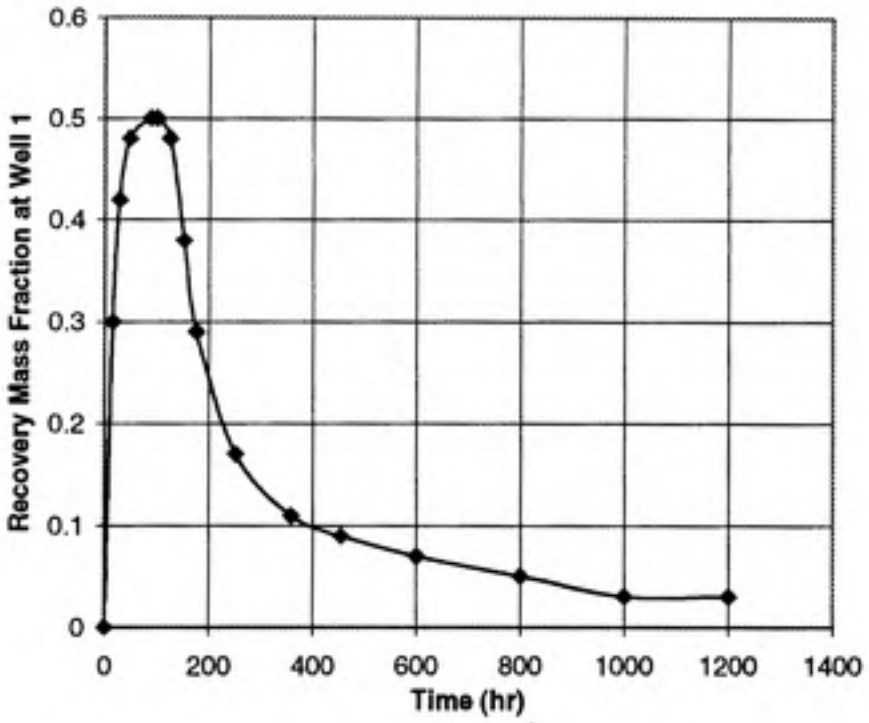

Figure 4.2 shows recovery mass fraction increasing during injection to a maximum value of 0.5, and this inflection point of the curve coincides with establishment of the density barrier and cessation of brine injection. The withdrawal rate for Well 1 was constant for the simulation represented in Figure 4.2; therefore the area under the curve is proportional to the total mass recovered and, by association, to the total mass injected. Referring to Figure 4.2 to illustrate DERD efficiency objectives, it is clear that the dual goals of efficient injection of brine for maximal effect and recovery of brine at the highest possible concentrations are enhanced when the mass diagram is compressed about the maximum mass fraction and the recovery tail is short and steeply inclined.

4.4 Simulation Formulation

The simulations were grouped according to the decision variable under evaluation, and all of the simulations performed for this report are summarized in Table 4.3.

Table 4.3 – Simulation Summary

Label	Sim	log k	Q1 (m^3/hr)	Q2 (m^3/hr)	Q3 (m^3/hr)	Q1'	Q2'	Q3'	a_L (m/s)	a_T (m/s)	A_1 (m^2)	A_2 (m^2)	A_1'	A_2'
Group 1, Set 1	s1	-10	20	100	100	1.0	0.2	0.0064	0.5	0.05	400	1600	2.5E-13	4
	s25	-10	24	120	120	1.0	0.2	0.0076	0.5	0.05	400	1600	2.5E-13	4
	s26	-10	30	150	150	1.0	0.2	0.0096	0.5	0.05	400	1600	2.5E-13	4
	s27	-10	36	180	180	1.0	0.2	0.0115	0.5	0.05	400	1600	2.5E-13	4
Group 1, Set 2	a1s4	-10	20	100	100	1.0	0.2	0.0038	0.5	0.05	676	2704	1.5E-13	4
	s12	-10	24	120	120	1.0	0.2	0.0045	0.5	0.05	676	2704	1.5E-13	4
	s19	-10	16	80	80	1.0	0.2	0.0030	0.5	0.05	676	2704	1.5E-13	4
	s22	-10	28	140	140	1.0	0.2	0.0053	0.5	0.05	676	2704	1.5E-13	4
	s24	-10	32	160	160	1.0	0.2	0.0060	0.5	0.05	676	2704	1.5E-13	4
	s28	-10	36	180	180	1.0	0.2	0.0068	0.5	0.05	676	2704	1.5E-13	4
	s29	-10	40	200	200	1	0.2	0.00754	0.5	0.05	676	2704	1.5E-13	4
Group 1, Set 3	s2	-10	20	100	100	1.0	0.2	0.0028	0.5	0.05	900	3600	1.1E-13	4
	s7	-10	30	150	150	1.0	0.2	0.0042	0.5	0.05	900	3600	1.1E-13	4
	s8	-10	16	80	80	1.0	0.2	0.0023	0.5	0.05	900	3600	1.1E-13	4
	s9	-10	40	200	200	1.0	0.2	0.0057	0.5	0.05	900	3600	1.1E-13	4
	s10	-10	35	175	175	1.0	0.2	0.0050	0.5	0.05	900	3600	1.1E-13	4
	s11	-10	32	160	160	1.0	0.2	0.0045	0.5	0.05	900	3600	1.1E-13	4
	s13	-10	48	240	240	1.0	0.2	0.0068	0.5	0.05	900	3600	1.1E-13	4
	s21	-10	24	120	120	1.0	0.2	0.0034	0.5	0.05	900	3600	1.1E-13	4
	s23	-10	28	140	140	1.0	0.2	0.0040	0.5	0.05	900	3600	1.1E-13	4

Table 4.3 – Simulation Summary (cont.)

Label	Sim	log k	Q1 (m^3/hr)	Q2 (m^3/hr)	Q3 (m^3/hr)	Q1'	Q2'	Q3'	a_L (m/s)	a_T (m/s)	A_1 (m^2)	A_2 (m^2)	A_1'	A_2'
Group 1, Set 4	s3	-10	20	100	100	1.0	0.2	0.0016	0.5	0.05	1600	6400	6.3E-14	4
	s14	-10	40	200	200	1.0	0.2	0.0032	0.5	0.05	1600	6400	6.3E-14	4
	s15	-10	48	240	240	1.0	0.2	0.0038	0.5	0.05	1600	6400	6.3E-14	4
	s16	-10	32	160	160	1.0	0.2	0.0025	0.5	0.05	1600	6400	6.3E-14	4
	s17	-10	35	175	175	1.0	0.2	0.0028	0.5	0.05	1600	6400	6.3E-14	4
	s20	-10	24	120	120	1.0	0.2	0.0019	0.5	0.05	1600	6400	6.3E-14	4
	s22	-10	28	140	140	1.0	0.2	0.0022	0.5	0.05	1600	6400	6.3E-14	4
Group 2	q1	-10		45	87	0.5		0.0055	0.5	0.05	400	1600	2.5E-13	4
	q3	-10		101	125	0.8		0.0080	0.5	0.05	400	1600	2.5E-13	4
	q4	-10	24	96	120	0.8	0.2	0.0076	0.5	0.05	400	1600	2.5E-13	4
	q5	-10	20	64	116	0.6	0.2	0.0074	0.5	0.05	400	1600	2.5E-13	4
	q6	-10		112	124	0.9		0.0079	0.5	0.05	400	1600	2.5E-13	4
	l1	-10		124	178	0.7		0.0113	0.5	0.05	400	1600	2.5E-13	4
	l2	-10	30	160	110	1.5	0.3	0.0070	0.5	0.05	400	1600	2.5E-13	4
	r1	-10	24	80	120	0.7	0.2	0.0076	0.5	0.05	400	1600	2.5E-13	4
Group 3	t4	-12		1.4	2	0.7		0.0128	0.5	0.05	400	1600	2.5E-15	4
	t5	-12	0.3	1.5	1.5	1.0	0.2	0.0096	0.5	0.05	400	1600	2.5E-15	4
	t6	-12	0.2	1	1	1.0	0.2	0.0064	0.5	0.05	400	1600	2.5E-15	4
	t7	-12	0.36	1.8	1.8	1.0	0.2	0.0115	0.5	0.05	400	1600	2.5E-15	4
	t8	-12		2	2.6	0.8		0.0167	0.5	0.05	400	1600	2.5E-15	4
Group 4	p1	-10		38	107	0.4		0.0068	0.5	0.05	400	1600	2.5E-13	4
	p3	-10		252	269	0.9		0.0171	0.5	0.05	400	1600	2.5E-13	4
	p6	-10		67	128	0.5		0.0082	0.5	0.05	400	1600	2.5E-13	4
Group 5	d1	-10	24	82	120	0.7	0.2	0.0076	0	0	400	1600	2.5E-13	4

4.4.1 Group 1 Simulations

The Group 1 simulations were formulated to examine the effects on DERD efficiency of

1. varying the total production rate (Q3) for a given area A1 and a constant 1:1 ratio of total injection to total production (Q3'); and

2. varying the size of area A1.

There are a total of 27 simulations in Group 1, separated into four sets according to A1 value. Within each set, A1 was held constant, and simulations were performed for different Q3 rates. In all Group 1 simulations, the production wells had equal pumping rates, resulting in a Q2' ratio of 0.2.

In all of the Group 1 simulations, the production wells were started prior to the injection wells to lower the water table. It should be noted that this strategy is perhaps too aggressive for some situations since some DNAPL mobilization will occur prior to establishment of the density barrier as a result of dewatering. In all of the Group 1 simulations, the domain is a homogeneous isotropic media with a permeability of 10^{-10} m^2.

In the Group 1, Set 1 simulations, the injection wells are spaced 20 meters apart resulting in a A1 of 400 m^2, as indicated in Table 4.3, and four simulations were performed at Q3 values of 100, 120, 150, and 180 m^3/hr, resulting in Q3' values ranging from 0.0064 to 0.0115. The objective function for all simulations was calculated as described in section 3.1, and a typical example of a simulation cost spreadsheet is shown in Table 4.4. The cost spreadsheets for all other simulations are stored on the compact disk included with this report.

Table 4.4 – Simulation s1 Cost Spreadsheet

Time (hr)	w mass frac.	w_{avg} well 1	Mass Recovered well 1 (kg)	Recovery Cost well 1	w wells 6-9	w_{avg} wells 6-9	Mass Recovered wells 6-9 (kg each)	Recovery Cost wells 6-9	% of mass recovered All wells	Total recovery cost All wells
200	0		0		0				0	0
215	0.3	0.15	5.19E+04	$ 7,256	0.17	0.09	2.10E+04	$ 4,782	2%	$ 26,386
227	0.42	0.36	1.81E+05	$ 2,583	0.29	0.23	9.33E+04	$ 4,512	7%	$ 47,018
247	0.48	0.45	4.63E+05	$ 2,859	0.36	0.33	2.80E+05	$ 4,721	20%	$ 68,761
287	0.5	0.49	1.09E+06	$ -	0.40	0.38	7.29E+05	$ 8,031	50%	$100,886
300	0.5	0.50	1.30E+06	$ -	0.50	0.45	8.87E+05	$ 1,602	61%	$107,293
324	0.48	0.49	1.68E+06	$ 584				$23,649	65%	$107,877
351	0.38	0.43	2.04E+06	$ 4,639		Total cost			70%	$112,516
376	0.29	0.34	2.27E+06	$ 5,405		wells 6-9		$94,595	73%	$117,921
451	0.17	0.23	2.68E+06	$ 25,589					78%	$143,509
558	0.11	0.14	3.03E+06	$ 53,761					82%	$197,270
655	0.09	0.10	3.24E+06	$ 46,137					85%	$243,407
800	0.07	0.08	3.48E+06	$ 58,049					88%	$301,457
1000	0.05	0.06	3.72E+06	$107,637					91%	$409,094
1200	0.03	0.04	3.88E+06	$ 94,642					93%	$503,736
1400	0.03	0.03	4.00E+06	$ 97,716					94%	$601,451
				$506,857						

Summary

Total mass recover	7.55E+06	kg
Total Mass injected	7.99E+06	kg
Percent recovery	0.94	
Capital Cost	$ 4,154,800	
Recovery Cost	$ 601,451	
Salvage Value	$ 3,170,160	
Total brine cost	**$ 1,586,091**	
Area treated	850 m^2 =	0.21 acres
Cost per acre	**$ 7,551,661**	

The typical density barrier coverage (area covered by a brine layer of minimum density 1550 kg/m^3) was an octagonal shaped area with boundaries lying between the injection well perimeter and the outer perimeter of production wells. Figure 4.3, which illustrates the limits of density barrier coverage for Simulation s1, is representative of the density barrier shape, and the extent of area coverage for each simulation was influenced by the total injection rate and the ratio of total injection rate to total production rate. Generally the higher the injection rate, the nearer the barrier limits were to the outer perimeter production wells. Hence different pumping strategies produced different density barrier limits for simulations in which all other variables were identical.

Figure 4.3 – Simulation s1 Limits of Density Barrier

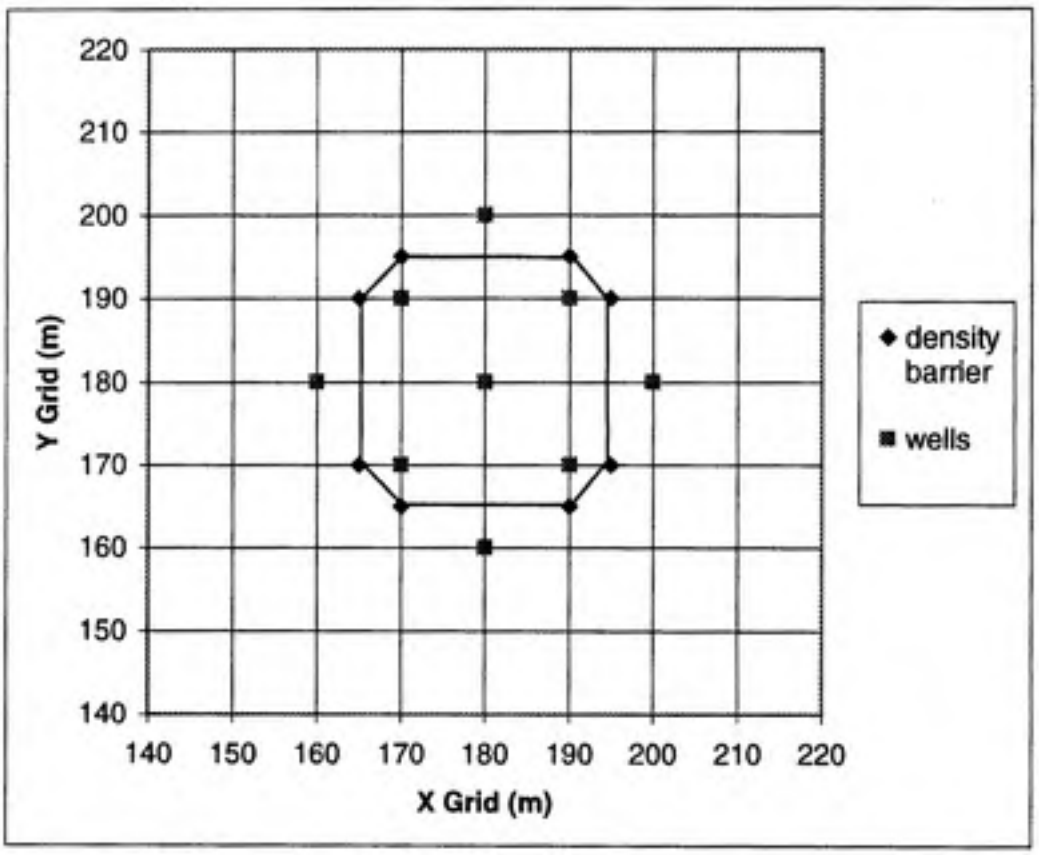

In the Group 1 / Set 2 simulations, summarized in Table 4.3, the injection wells were spaced 26 meters apart resulting in an A1 area equal to 676 m^2, and seven simulations were performed at Q3 rates ranging from 80 to 200 m3/hr. In the Group 1 / Set 3 simulations, the injection wells were spaced 30 meters apart resulting in A1 equal to 900 m^2, and nine simulations were performed at Q3 rates from 80 to 240 m^3/hr. In the Group 1 / Set 4 simulations, the injection wells were spaced at 40 meters resulting in an A1 of 1600 m^2, and six simulations were performed at Q3 values ranging from 100 to 200 m^3/hr.

The brine unit costs (objective function) for the Group 1 simulations are summarized in Tables 4.5, 4.6, 4.7, and 4.8, and are depicted graphically in Figure 4.3.

Table 4.5 – Group 1 / Set 1 Brine Unit Costs

Sim	A1 (m^2)	A1'	Q3 (m^3/hr)	Q3'	Area Treated (m^2)	Cost per acre ($M)
s1	400	3E-13	100	0.0064	850	7.55
s25	400	3E-13	120	0.0076	850	5.29
s26	400	3E-13	150	0.0096	850	5.01
s27	400	3E-13	180	0.0115	900	7.85

Table 4.6 – Group 1 / Set 2 Brine Unit Costs

Sim	A1 (m^2)	A1'	Q3 (m^3/hr)	Q3'	Area Treated (m^2)	Cost per acre ($M)
a1s4	676	1.5E-13	80	0.0030	900	6.39
s12	676	1.5E-13	100	0.0038	900	8.15
s19	676	1.5E-13	120	0.0045	1550	11.89
s22	676	1.5E-13	140	0.0053	1550	5.84
s24	676	1.5E-13	160	0.0060	1550	5.08
s28	676	1.5E-13	180	0.0068	1550	4.82
s29	676	1.5E-13	200	0.0075	1600	5.17

Table 4.7 – Group 1 / Set 3 Brine Unit Costs

Sim	A1 (m^2)	A1'	Q3 (m^3/hr)	Q3'	Area Treated (m^2)	Cost per acre ($M)
s8	900	1.1E-13	80	0.0023	1550	7.73
s2	900	1.1E-13	100	0.0028	1550	5.27
s21	900	1.1E-13	120	0.0034	1600	5.93
s23	900	1.1E-13	140	0.0040	2450	4.74
s7	900	1.1E-13	150	0.0042	2450	4.26
s11	900	1.1E-13	160	0.0045	2450	4.14
s10	900	1.1E-13	175	0.0050	2450	4.13
s9	900	1.1E-13	200	0.0057	2450	3.83
s13	900	1.1E-13	240	0.0068	2450	4.35

Table 4.8 – Group 1 / Set 4 Brine Unit Costs

Sim	A1 (m^2)	A1'	Q3 (m^3/hr)	Q3'	Area Treated (m^2)	Cost per acre ($M)
s3	1600	6.3E-14	100	0.0016	2450	8.23
s18	1600	6.3E-14	120	0.0019	4175	9.10
s16	1600	6.3E-14	160	0.0025	3775	5.26
s17	1600	6.3E-14	175	0.0028	3775	4.57
s14	1600	6.3E-14	200	0.0032	4450	3.93
s15	1600	6.3E-14	240	0.0038	4450	4.21

Figure 4.4 – Group 1 Brine Unit Costs

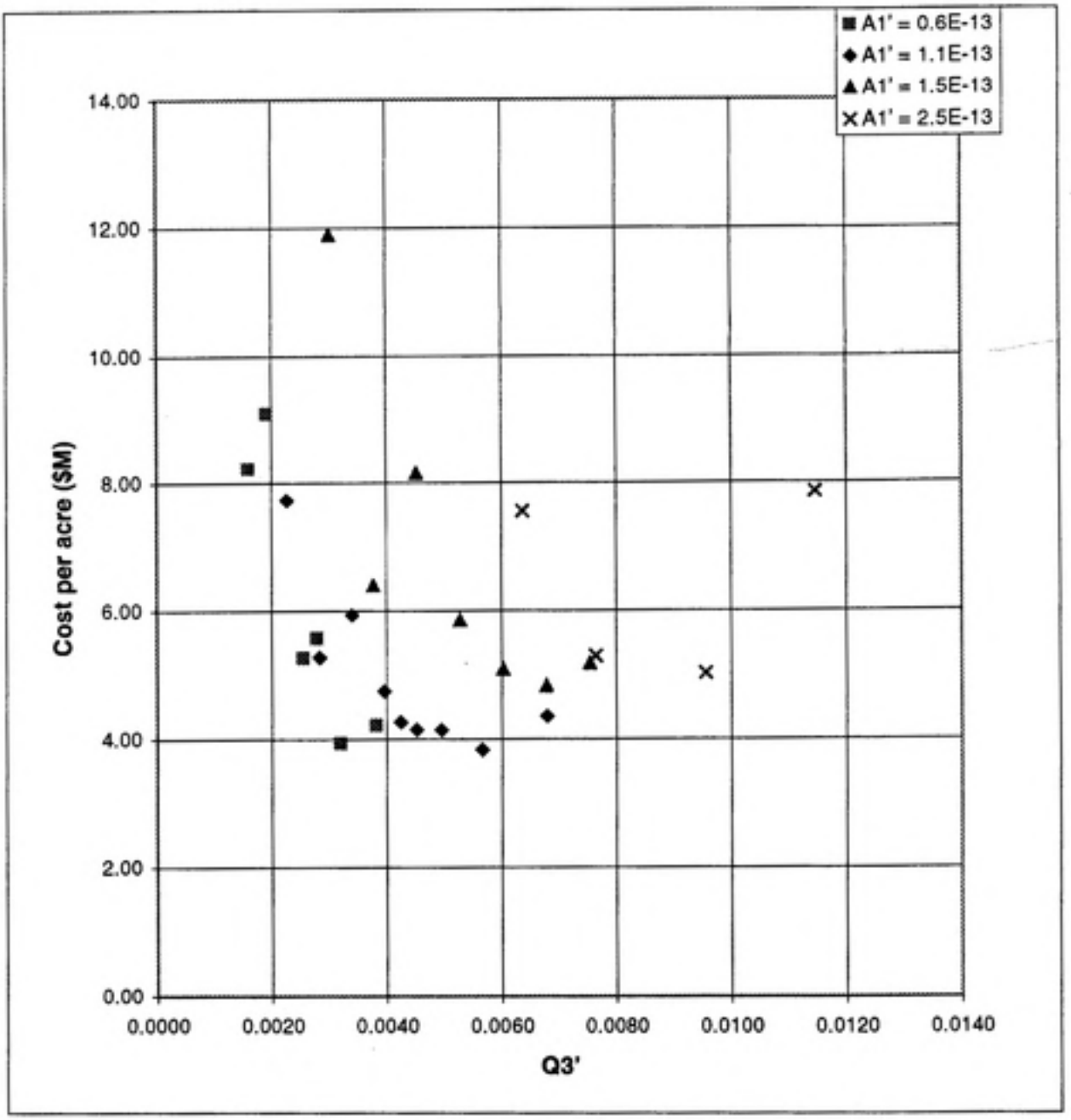

Examination of Figure 4.4 suggests that for a given injection well perimeter area, A1, there exists an optimal range of Q3' that minimizes brine unit costs. All of the curves exhibit high unit costs at the low end of Q3', and then decline sharply before plateauing or even becoming convex as Q3' increases.

Tables 4.5 through 4.8 and Figure 4.4 illustrate the sensitivity of brine unit cost to the size of the treated area, or density barrier coverage. Anomalies in the apparent unit cost-Q3' relationship occurred in some ranges of Q3' through which there was a transition in area treated, e.g. between Q3 rates of 100 to 140 m^3/hr in the Set 2 Simulations (Table 4.6). The increase in Q3 from 100 to 120 m^3/hr, Simulation a1s4 to Simulation s12, resulted in a spike in unit cost as the area treated increased from 900 to 1550 m^2. The unit cost-Q3' curve is again decreasing between Q3 rates of 120 and 140 m^3/hr (Simulation s12 to Simulation s22). Such discontinuities indicate that operation at some Q3' transitional values can be inefficient.

The brine unit cost results also demonstrate how engineering judgment in deciding when to stop the injection stage can affect the size of density barrier coverage and the efficiency of the process. Simulation s18 with a Q3 rate of 120 m^3/hr (Table 4.8) was continued until the treated area reached 4175 m^2. This simulation, which is bracketed by simulations with treated areas of 2450 and 3775 m^2 and Q3 rates of 100 and 160 m^3/hr respectively, resulted in a significantly higher unit cost than either of the adjacent simulations.

Some of the unit cost-Q3' curves appear to be cut off before a full pattern of behavior at the high end of the range of Q3 rates is established. This occurred because Q3 rates beyond the limits of the curves are impractically high for the given well spacing and aquifer depth. In Figure 4.3, the simulation sets with larger A1 areas seemed to result in slightly lower optimal unit cost ranges. This apparent trend could be due to greater sensitivity of cost per acre calculations to area measurement and the increased error in measuring brine coverage in the simulations with smaller A1s. Since the density reported at each node in the HST3D results is the average density in the cell volume assigned to the node, there is some error in estimating the true density barrier coverage for each simulation, and the relative magnitude of this error increases as area decreases. An error of 1 meter on each side in estimating the true dimensions of the barrier limits results in a

14% error in area measurement for an 850 m^2 density coverage (typical of Set 1) compared to a 6% error for the 4450 m^2 density coverage (Set 4).

The Set 1 results seem to indicate that process inefficiencies are encountered when Q3 rates fall either too far below or too far above the optimal range. Figure 4.5 shows that more than one-and-a-half times solute mass was required per acre treated for the low end (S1) and the high end (S27) Q3 simulations than for either of the two simulations in the optimal Q3 range (S25 and S26).

Figure 4.5 – Group 1, Set 1 Total Mass of Solute Injected per Acre of Area Treated

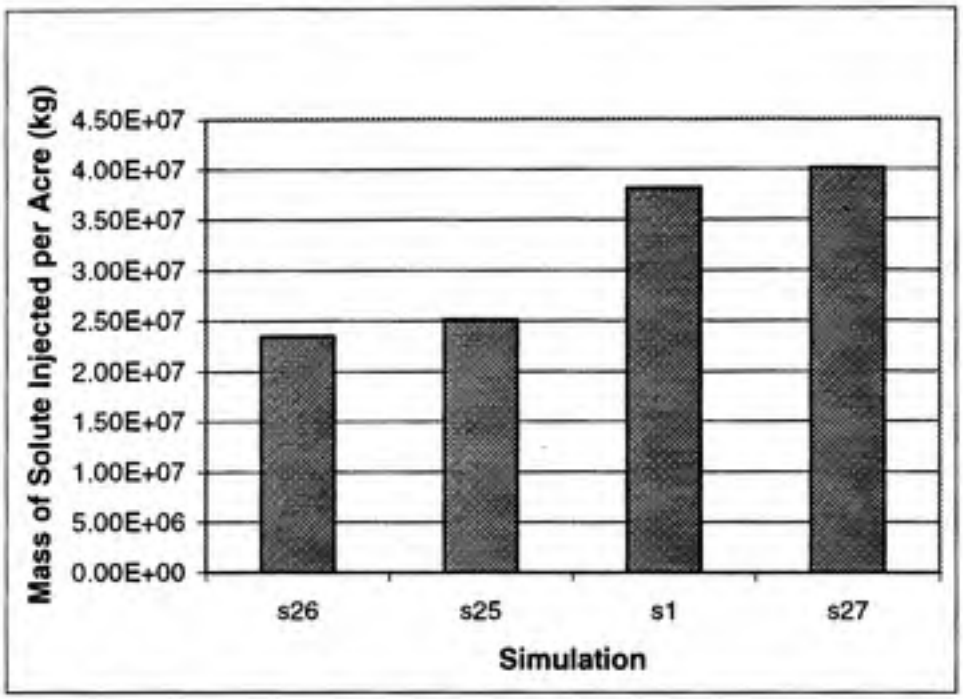

Figure 4.6 depicts total mass of solute recovered plotted against time for the Set 1 simulations to illustrate the behavior of both density barrier development and brine recovery. The linear segment of the curves in which rate of mass recovery is high represents the mass injection stage, and the end of the straight line portion where the curve becomes convex marks full development of the density barrier and the consequent cessation of injection.

Figure 4.6 - Group 1 / Set 1 Total Mass Solute Recovered vs. Time

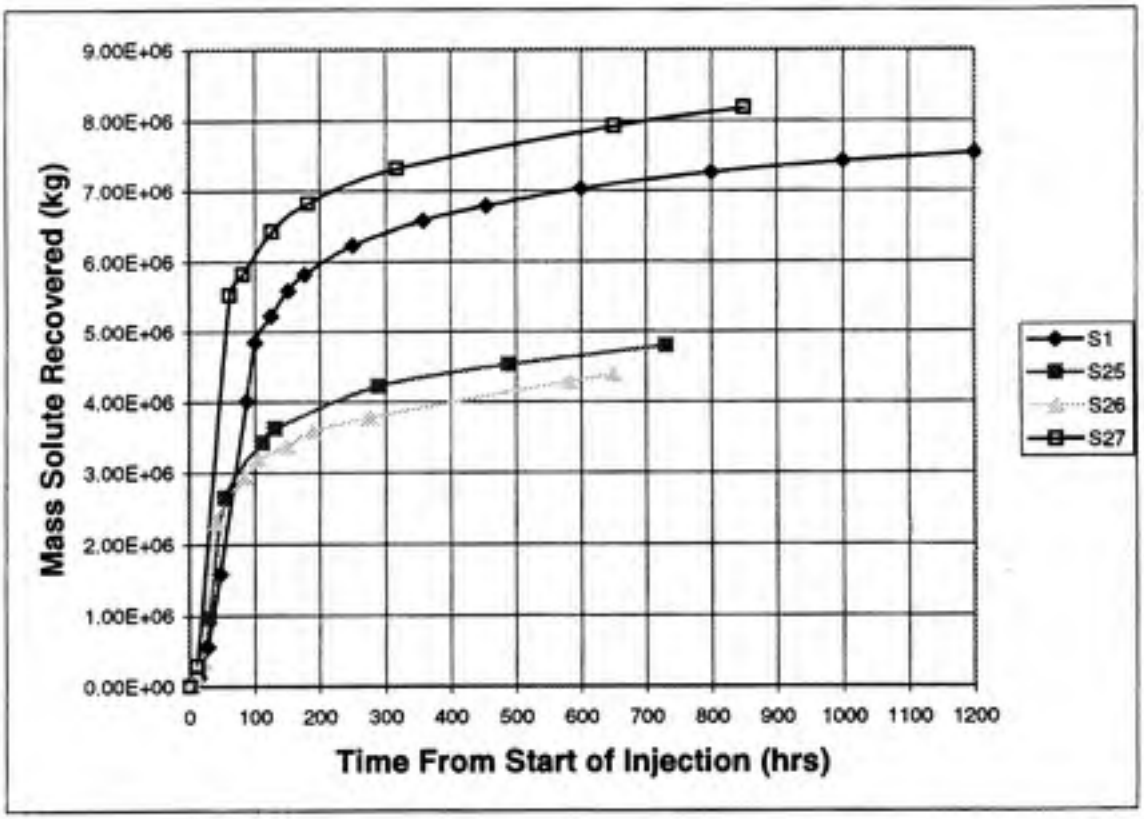

In the low and high Q3 simulations, s1 and s27, more than 60% of the total mass of solute injected was recovered prior to density barrier development, compared to 50% for the two simulations in the optimal Q3 range. The mass of brine recovered prior to development of the density barrier essentially has been cycled through the domain without contributing to the final brine layer volume. Therefore as this percentage increases, more brine is injected per area treated and brine injection efficiency decreases.

The Set 1 results seem to indicate that for Q3' ratios significantly lower than the optimal range, the total injection rate, Q2, which is equal to Q3, is not high enough to establish the required densities without significant loss of solute through the production wells. Conversely increasing Q3' ratios above the optimal range seems to cause solute to

be pulled through the production wells at too high a rate for efficient establishment of the brine layer.

4.4.1 Group 2 Simulations

The Group 2 simulations were formulated to evaluate the effects of the following pumping strategies on DERD efficiency:

- varying the ratio of total injection rate to total production rate (dimensionless parameter Q1') with Q2 and Q3 constant in time;
- varying Q2 and Q3 rates with time and in Q1' ratios that varied with time;
- beginning injection with production, i.e. without preliminary lowering of the water table; and
- using Wells 1 through 5 in second stage brine recovery as opposed to Well 1 alone.

The nine simulations performed for Group 2 are summarized in Table 4.9 below. In all of the Group 2 simulations, except r1 and r1a, the region was partially dewatered by the production wells prior to brine injection. Brine injection was then initiated slowly in Q1' ratios designed to maintain a lowered water table and thereby minimize the quantity of brine required. Although this strategy was effective in minimizing the mass of brine required to establish the density barrier, such a practice may be too aggressive for some site applications due to the risk of DNAPL migration prior to establishment of the density barrier. Using a more conservative approach in simulations r1 and r1a, injection was initiated with production in gradually increasing Q1' ratios designed to develop the density barrier as the water table was lowered.

Table 4.9 – Group 2 Simulations

Simulation	Q2 (m3/hr)	Q3 (m3/hr)	Q2/Q3 (Q1')
q4	Constant at 96	Constant at 120	0.80
q5	Constant at 64	Constant at 116	0.55
l2	Constant at 160	Constant at 110	1.45
q1	Varied, Avg. 45	Varied, Avg. 91	Avg. 0.49
q3	Varied, Avg. 92	Varied, Avg. 113	Avg. 0.81
q6	Varied, Avg. 96	Varied, Avg. 107	Avg. 0.90
l1	Varied, Avg. 98	Varied, Avg. 141	Avg. 0.70
r1	Varied, Avg. 80	Constant at 120	Avg. 0.67
r1a	Varied, Avg. 80	Constant at 120	Avg. 0.67

In simulations q4, q5, and l2, Q2 and Q3 rates were held constant to examine the effect of different constant Q1' values. In simulations q1, q3, q6, and l1, Q2 and Q3 rates and Q1' ratios were varied with time, and time weighted average values are reported in Table 4.9. In simulation r1, the preliminary drawdown stage was eliminated, Q3 was held constant, and the Q2 rate and Q1' ratio varied with time. Simulation r1a is a variation of Simulation r1 performed to evaluate the effect of withdrawing brine from Wells 1 through 5 rather than Well 1 alone and is identical to simulation r1 up the brine withdrawal stage. A1 was held constant at 400 m^2 for all Group 2 simulations, so comparisons may also be drawn to the Group 1 / Set 1 simulations in which A1 was 400 m^2, but Q1' was constant at 1.0.

Figures 4.6 to 4.10 show how Q2 and Q3 rates varied with time for Simulations q1, q3, q6, l1, r1 and r1a, from the beginning of injection to the establishment of the density barrier.

Figure 4.7 – Simulation q1 Total Injection and Production Rates vs. Time

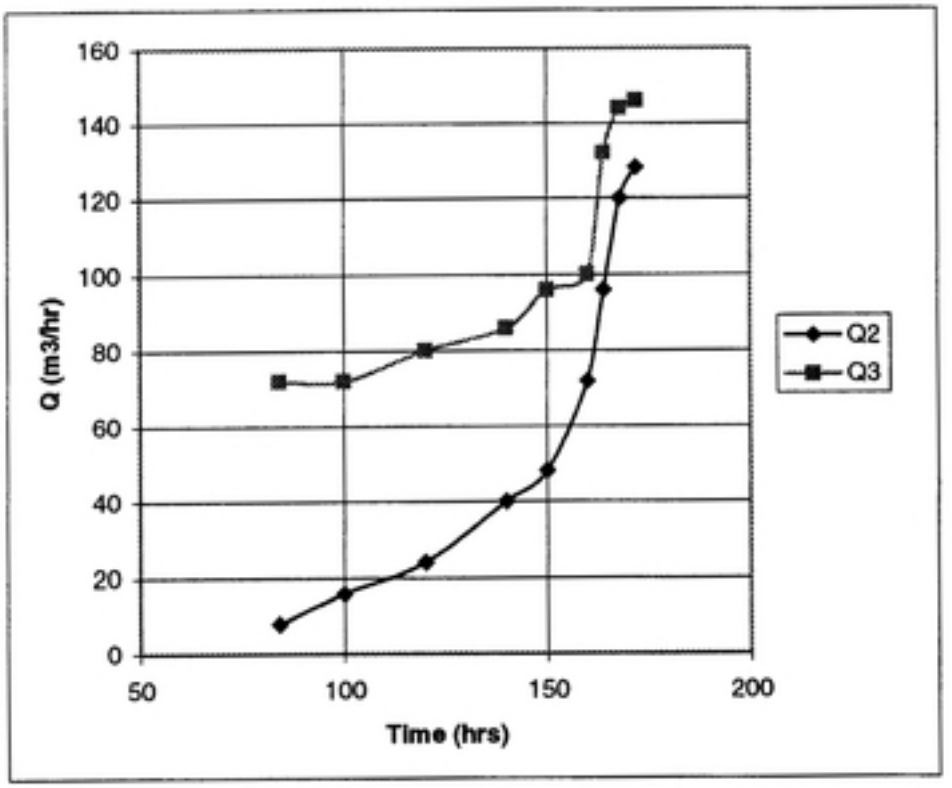

Figure 4.8 – Simulation q3 Total Injection and Production Rates vs. Time

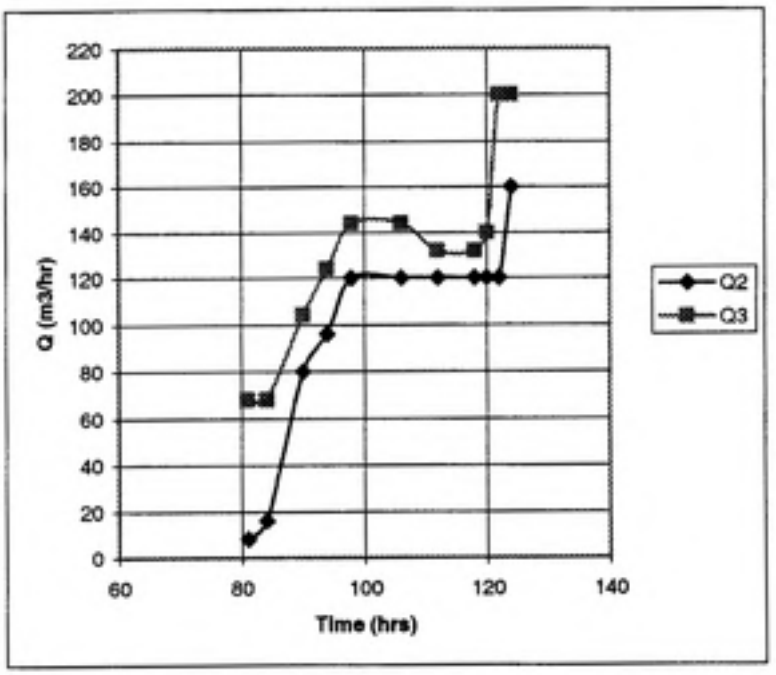

Figure 4.9 – Simulation q6 Total Injection and Production Rates vs. Time

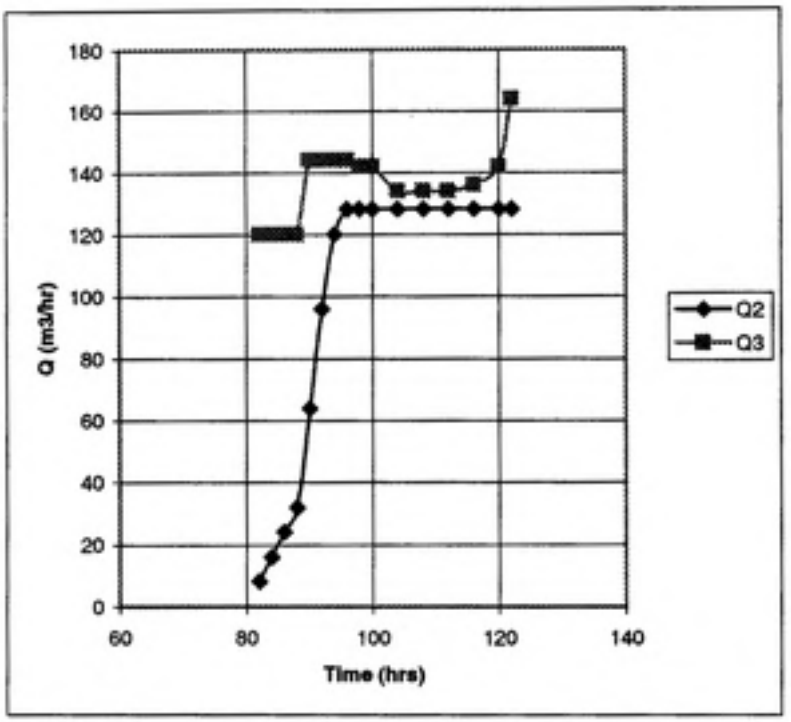

Figure 4.10 – Simulation 11 Injection and Production Rates vs. Time

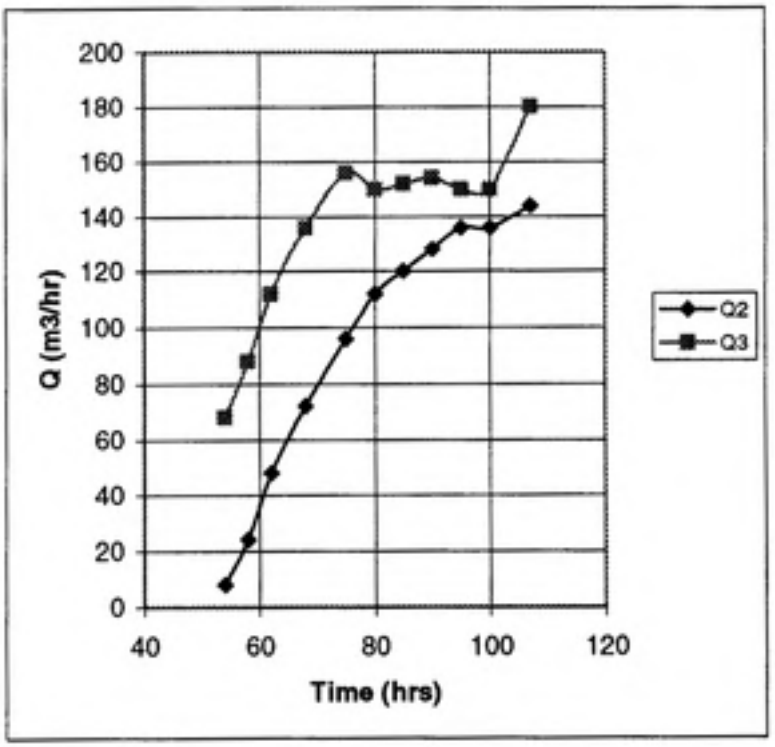

Figure 4.11 – Simulations r1 and r1a Injection and Production Rates vs. Time

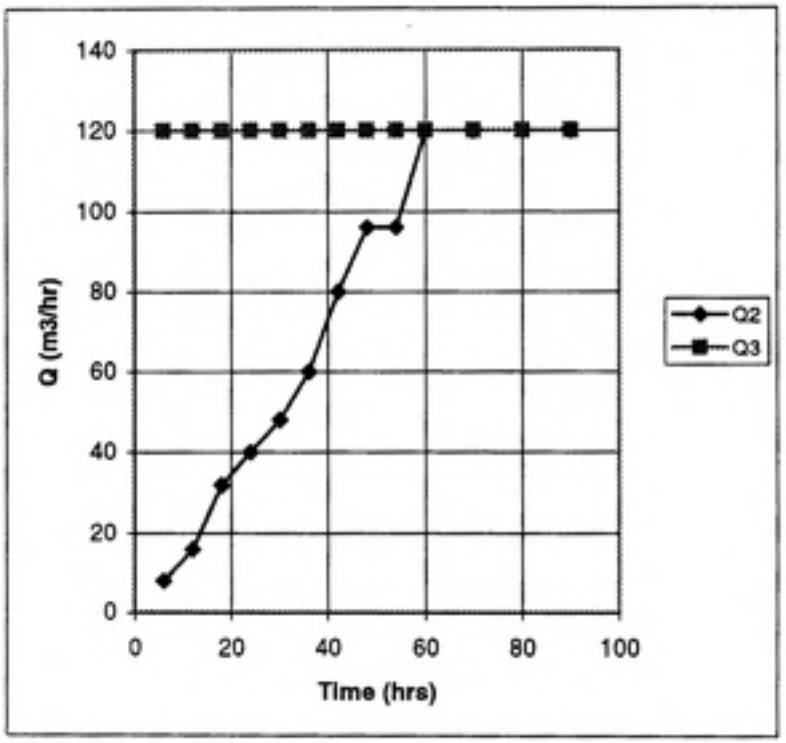

The results of the Group 2 simulations are summarized in Table 4.10, and Figure 4.12 illustrates the total mass of solute injected per acre of density barrier coverage for the Group 2 simulations with the simulations listed in order of ascending unit cost. Simulation s25 from Group 1 was included in Table 4.10 and Figure 4.12 for comparison purposes.

Table 4.10 – Group 2 Simulation Summary

Col (1) Sim	Col (2) Q2 (m^3/h)	Col (3) Q3 (m^3/h)	Col (4) Q1'	Col (5) Total Mass Solute Injected (kg)	Col (6) Total Mass Solute in Barrier after injection (kg)	Col (7) % Mass in Barrier after Injection	Col (8) Area Treated (m^2)	Col (9) Total Mass injected per area treated (kg/ac)	Col (10) Mass in barrier per area treated (kg/ac)	Col (11) Cost per Acre ($M)
q6	96	107	0.90	3.32E+06	1.83E+06	55%	850	1.58E+07	8.71E+06	3.11
q3	92	113	0.81	3.46E+06	1.76E+06	51%	850	1.65E+07	8.38E+06	3.28
l1	98	141	0.70	4.23E+06	1.86E+06	44%	850	2.01E+07	8.86E+06	3.82
q5	64	116	0.55	2.29E+06	1.17E+06	51%	400	2.32E+07	1.18E+07	5.63
q4	96	120	0.80	5.32E+06	2.07E+06	39%	700	3.08E+07	1.20E+07	5.93
s25	120	120	1.00	5.27E+06	2.64E+06	50%	850	2.51E+07	1.26E+07	5.29
l2	160	110	1.45	4.84E+06	3.19E+06	66%	850	2.30E+07	1.52E+07	5.06
r1	80	120	0.67	5.74E+06	2.75E+06	48%	850	2.73E+07	1.31E+07	6.17
r1a	80	120	0.67	5.74E+06	2.75E+06	48%	850	2.73E+07	1.31E+07	5.66

Figure 4.12 – Group 2 Solute Mass Injected per Acre Density Barrier Coverage (simulations listed in order of unit cost)

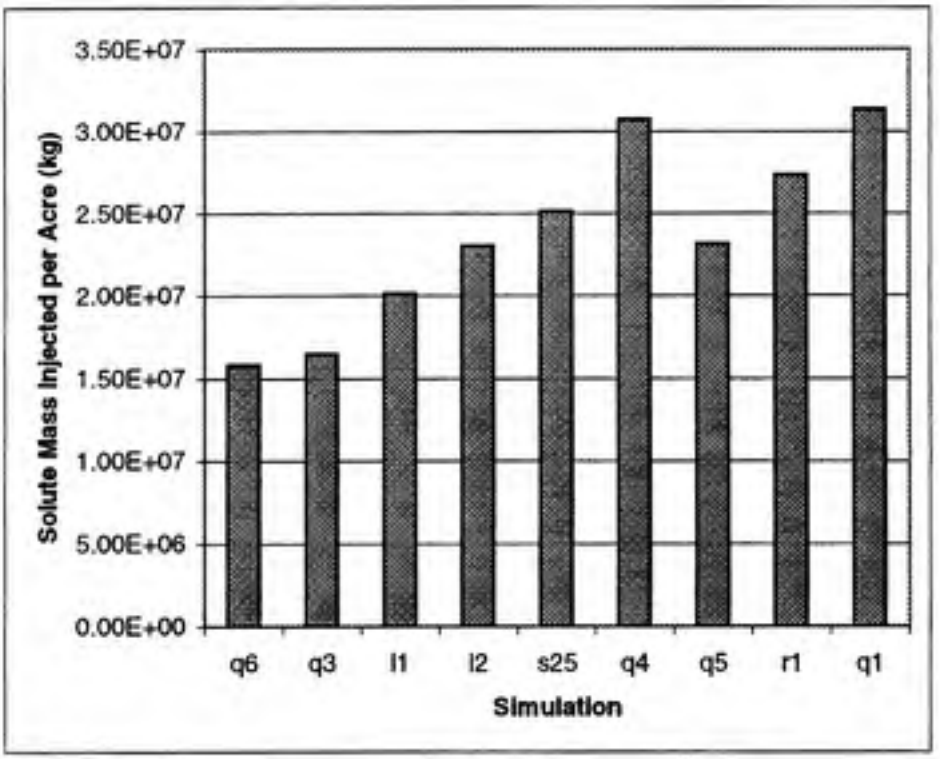

The simulations with the lowest unit cost and most efficient solute injection (Simulations q6, q3, and l1) were those in which Q2 and Q3 rates were varied with time to maintain lowered water table elevations throughout the density barrier development stage. In comparison to simulations with equivalent but constant Q2 and Q3 rates, Simulations q6 and q3 unit costs were 60% of the unit costs for Simulations s25 and q4 and required only 64% of the solute mass to cover the same area. Thus brine injection efficiency and unit cost can be improved by using variable pumping rates to control the water table elevation throughout the process.

Figures 4.7 and 4.8 show that Simulations q3 and q6 vary slightly with respect to early Q3 rates, which started more slowly in simulation q3, and in average Q1', which is slightly higher for simulation q6. The equivalence of the unit costs and solute mass used for the two simulations indicates that this variation had no significant impact on process

efficiency. In comparison, Figure 4.9 shows a wider gap between Q2 and Q3 for Simulation l1, which resulted in a lower average Q1' than either Simulation q3 or q6. While an equivalent mass of solute was in the barrier after injection (column 6 of Table 4.10), more total mass (column 5) was injected in Simulation l1 relative to q3 and q6, and l1 had a 12% higher unit cost.

Comparison of simulation r1 to Simulations q3, q6, q4, q5, l1, and l2 provides some insight into the effects of the preliminary drawdown stage, which was not included in simulation r1. Compared to the above simulations with preliminary drawdown

- The r1 unit cost was almost twice the cost of the three most efficient simulations (q3, q6, and l1), which had Q2, and Q3 rates that varied. The Q1' ratios in Simulations q6 and q3 were higher than Q1' for Simulation r1, but the Q1' in Simulation l1 was equivalent to that of Simulation r1. There was therefore a substantial difference in efficiency that was not attributable to Q1' ratio differences.

- The r1 unit cost was 20% greater than the unit cost for Simulations q4, s25, and l2, which had constant Q2 and Q3 rates and Q1' ratios of 0.80, 1.00, and 1.45 respectively.

- The r1 unit cost was comparable to the two simulations with the lowest Q1' ratios. Simulation q5 had constant Q2 and Q3 rates in a constant Q1' ratio of 0.55, and Simulation q1 had varied Q2 and Q3 rates and an average Q1' ratio of 0.49.

The above analysis suggests that the most efficient operation is achieved with preliminary drawdown followed by varied Q2 and Q3 rates in a ratio around 0.9. Simulations with preliminary drawdown and constant Q2 and Q3 rates in ratios from 0.80 to 1.45 (q4, s25, and l2) occupied the next tier of efficiency. The worst efficiency results occurred for simulations with low Q1' ratios, with either varied or constant pumping rates (q5 and q1), and for the simulation without preliminary drawdown (r1).

A variation of Simulation r1 (Simulation r1a) was performed to compare the results of brine recovery through the central well and the inner perimeter wells as opposed to the central well solely. Simulation r1a is identical to Simulation r1 through development of the density barrier, but at inception of the brine recovery stage Wells 1 through 5 each were given a production capacity of 10 m^3/hr, compared to a capacity of 20 m^3/hr in Well 1 alone for Simulation r1.

Distributing brine recovery across the area in five wells rather than one reduced the unit cost for the otherwise identical process from $6,170,000 per acre to $5,660,000 per acre. This modification, not only increased efficiency in terms of recovery mass fraction, but also reduced the total process time by half. Figure 4.13 illustrates total mass recovery plotted against time for simulations r1, and r1a.

Figure 4.13 – Total Solute Mass Recovered vs. Time

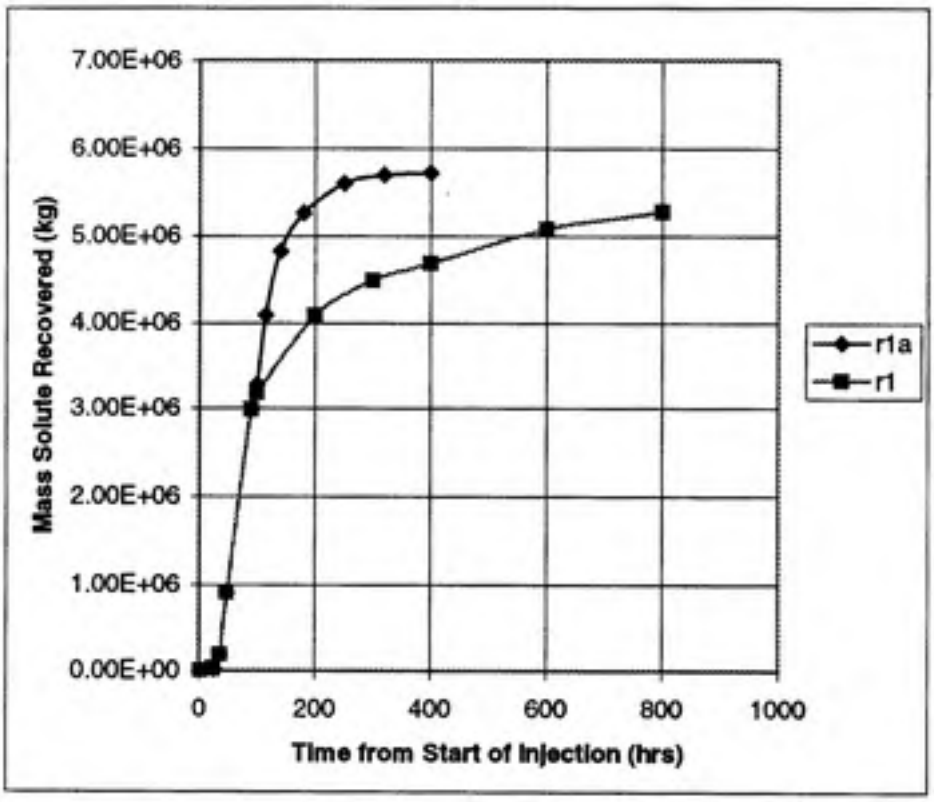

4.4.3 Group 3 Simulations

The Group 3 simulations were performed to evaluate the impact of a reduced porous medium permeability on DERD effectiveness. Five simulations were performed with an injection well spacing of 20 meters (A1 area equal to 400 m^2), and a soil permeability of 10^{-12} m^2. Hence the Group 3 simulations have the same well locations as the Group 1 / Set 1 and the Group 2 simulations but were performed with permeability two orders of magnitude less.

In Simulations t4 through t7, the water table was lowered prior to injection, and in Simulation t8, injection was initiated with production. Simulations t4 and t8 had time variable pumping rates, while Simulations t5, t6, and t7 had constant rates. The five Group 3 simulations are summarized in Table 4.11, and well flow rates are graphed against time for simulations t4 and t8 in Figures 4.14 and 4.15. The pumping rates in Simulations t4 and t8 were varied in response to water table fluctuations and fluid mass balances throughout the simulations to maintain partial drawdown of the water table.

All of the Group 3 simulations employed Wells 2 through 5 in the brine recovery stage after approximately 70 to 80% of the solute mass had been recovered.

Table 4.11 – Group 3 Simulations

Simulation	Description
t4	Water table lowered prior to injection Q2 and Q3 vary with time Avg Q2 = 1.4 m^3/hr Avg Q3 = 2.0 m^3/hr Avg Q1' = 0.7
t5	Water table lowered prior to injection (identical to t4) Q2 and Q3 are constant with time Q2 = 1.5 m^3/hr Q3 = 1.5 m^3/hr Q1' = 1.0
t6	Water table lowered prior to injection (identical to t4) Q2 and Q3 are constant with time Q2 = 1.0 m^3/hr Q3 = 1.0 m^3/hr Q1' = 1.0
t7	Water table lowered prior to injection (identical to t4) Q2 and Q3 are constant with time Q2 = 1.8 m^3/hr Q3 = 1.8 m^3/hr Q1' = 1.0
t8	Injection initiated with production Q2 and Q3 vary with time Avg Q2 = 2.0 m^3/hr Avg Q3 = 2.6 m^3/hr Avg Q1' = 0.8

Figure 4.14 – Simulation t4 Pumping Rates

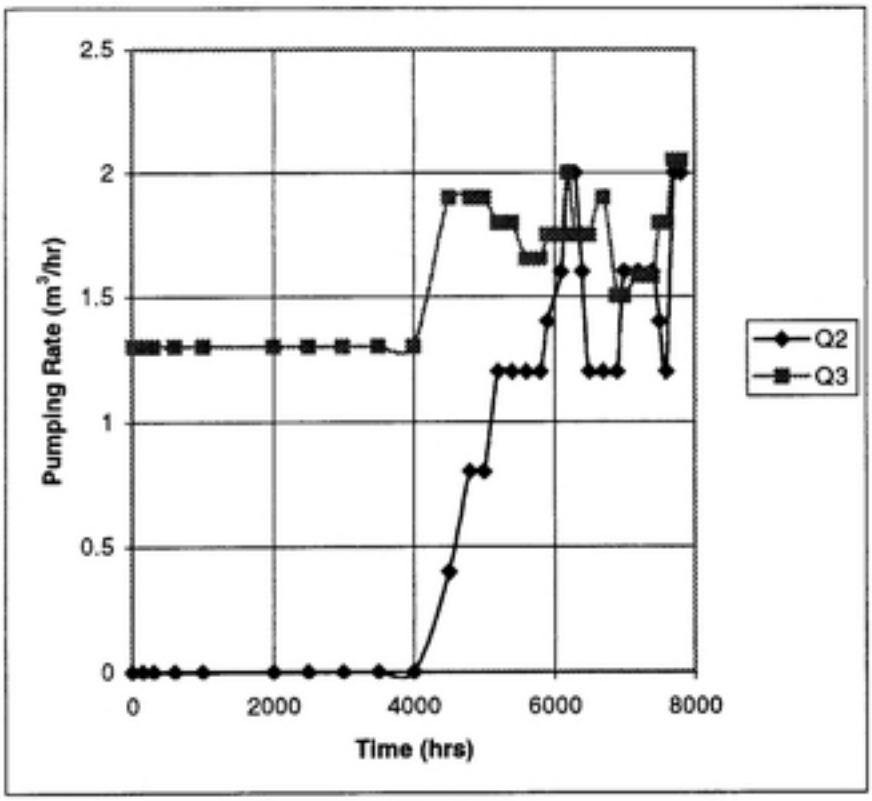

Figure 4.14 – Simulation t8 Pumping Rates

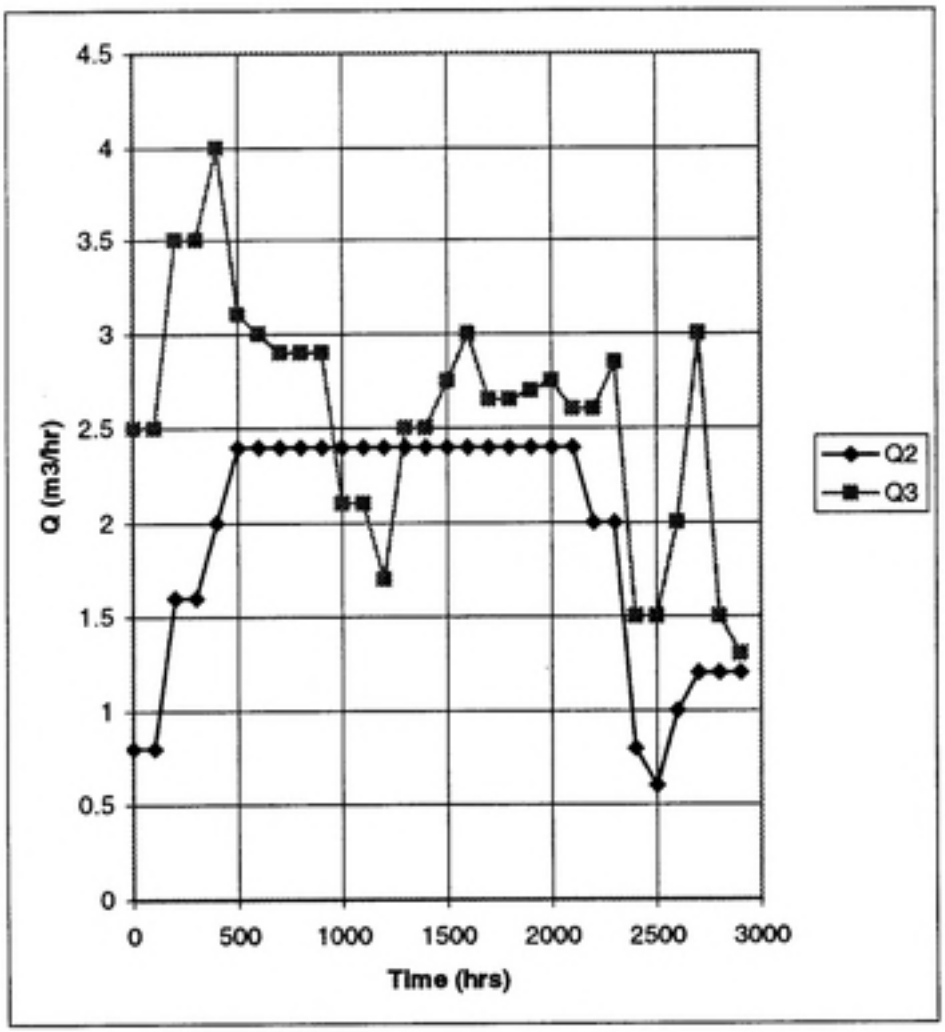

Table 4.12 and Figure 4.16 summarize the results of the Group 3 simulations. All of the Group 3 simulations resulted in a density barrier of 850 m^2 or 0.21 acre. Figure 4.17 presents unit cost plotted against Q3' for Group 3 compared to Group 1, Sets 1 and 2 simulations which have A1s of 400 and 676 m^2 respectively.

Table 4.12 – Group 3 Cost Summary

Sim	Q2	Q3	Mass Solute Injected	Mass in Region at w/d	Cost per acre
	(m^3/hr)	(m^3/hr)	(kg)	(kg)	($M)
t4	1.4	2.0	3.70E+06	1.85E+06	3.83
t5	1.5	1.5	4.79E+06	2.25E+06	4.82
t6	1.0	1.0	7.51E+06	4.13E+06	7.43
t7	1.8	1.8	4.30E+06	1.94E+06	4.19
t8	2.0	2.6	4.50E+06	2.39E+06	4.02

Figure 4.16 – Group 3 Unit Cost vs. Total Solute Mass Injected

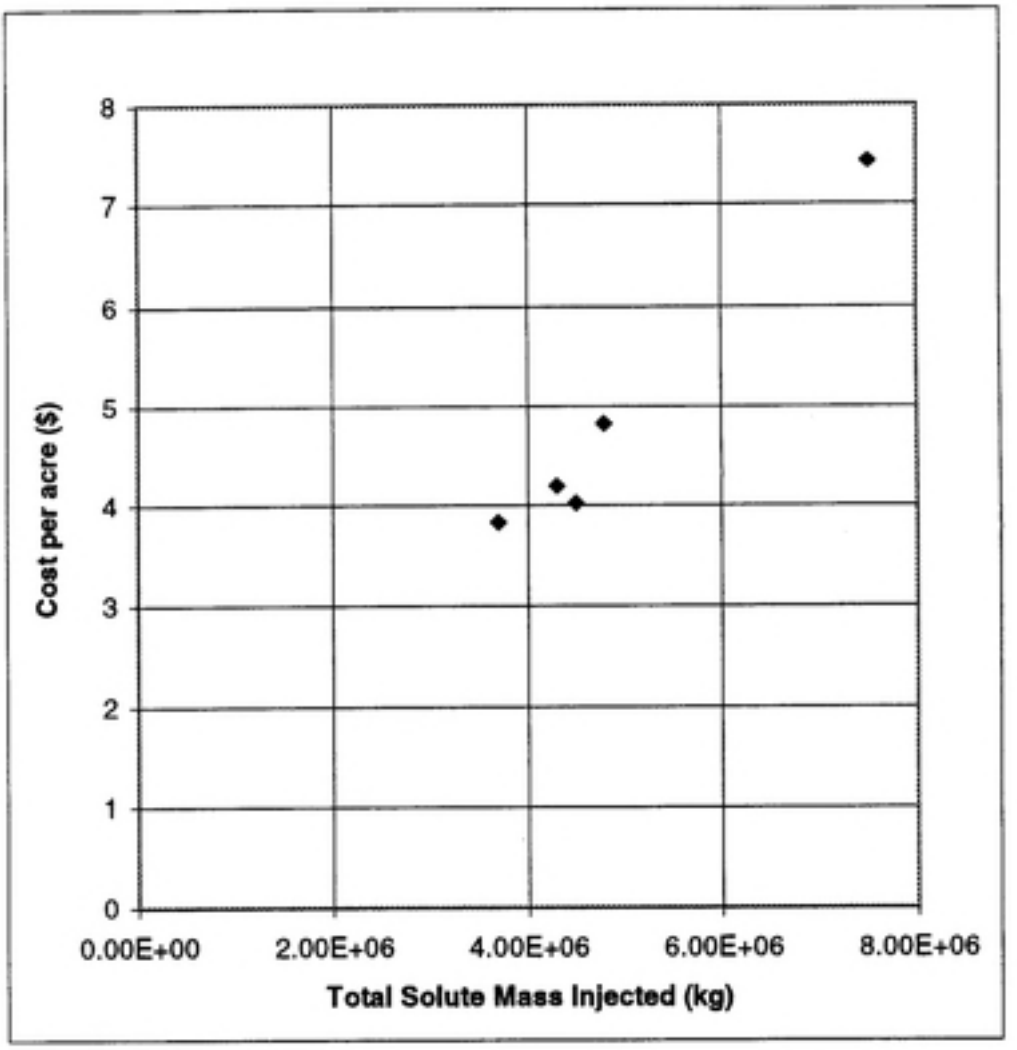

Figure 4.17 – Unit Cost vs. Q3' for Group 3 and Group1, Sets 1 and 2

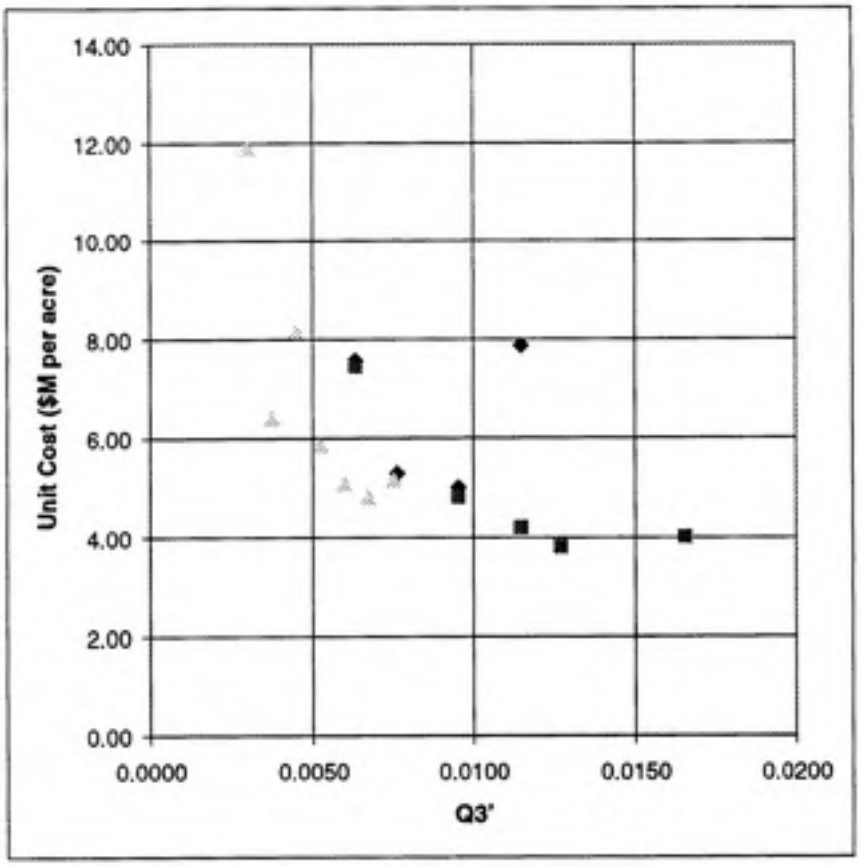

The following observations may be made in reference to Table 4.12 and Figures 4.15 and 4.16:

1. The Group 3 simulations exhibit a unit cost-Q3' curve similar to the Group 1 simulations. Unit costs are highest for the lowest Q3' values, then decline sharply before leveling in a region of optimal Q3'.

2. In the Group 3 simulations, elimination of preliminary drawdown, in Simulation t8, did not result in reduced efficiency or increased unit cost as was the case with the analogous Group 2 test. In the lower permeability medium, the time scale for water table fluctuations in response to pumping is much longer, and the rate and impact of fluid inflow resulting from regionally lowered water table elevations is much less.

3. The Group 3 simulation with the highest Q3', t8, required more mass solute than the simulation with the next highest Q3', simulation t7. Given this relationship, simulation t7 should have the lower unit cost if brine recovery occurs in identical fashion for the two simulations. The reason simulation t8 resulted in a slightly lower unit cost is a more efficient brine recovery stage. Production from Wells 2 to 5 was initiated earlier in simulation t8 (with 21% of the solute mass remaining) than in t7 (17%), and the results of the Group 2 simulations indicate increased efficiency when Wells 2 to 5 are used in brine recovery. A higher unit cost for t8 would indicate the start of an increasing unit cost-Q3' relationship, which would be congruent with the convex curves found in Group 1.

4. The unit cost-Q3' curves for Group 3 and Group 1 / Set 1 begin to diverge as Q3' increases. A comparison of simulation s27 to simulation t7, each with Q3' values of 0.012, shows that s27 required approximately twice as much solute mass and cost nearly twice as much. The reason for this difference in efficiency could be due to greater longitudinal dispersion in simulation s27, which has pore velocities two orders of magnitude greater than those in simulation t7. This greater smearing of the density front in s27 could result in more solute mass beyond the limits of the density barrier.

5. Comparisons of low and high permeability simulations at the lower end of the Q3' range, s1 to t6 and s26 to t5, reveal unit costs and solute mass utilizations that are equivalent.

6. The largest effect on the DERD process created by the lower permeability is the time required to complete the process. The Group 1 simulations required hundreds of hours compared to tens of thousands of hours for the Group 3 simulations.

4.4.4 Group 4 Simulations

A fourth group of simulations was performed to evaluate heterogeneity effects. In the three Group 4 simulations, the vertical plane of the domain was segmented into five one-meter thick strata each with a different soil permeability. Each of the three simulations had an average permeability of 10^{-10} m^2. The variance of permeability was 1.0 for simulations p1 and p6 and 0.5 for simulation p3. Simulation p6 was an inversion of the strata of simulation p1 to examine the effect of location of relative permeabilities. In simulation p1, the strata near the surface were more permeable than the lower strata, and in simulation p6 the order was inverted. The Group 4 media properties are summarized in Table 4.14.

Table 4.14 – Group 4 Permeabilities by Strata

	Simulation p1	Simulation p3	Simulation p6
Stratum Elevation (m)	Stratum Permeability (m^2)	Stratum Permeability (m^2)	Stratum Permeability (m^2)
4 – 5	$10^{-9.5}$	$10^{-11.0}$	$10^{-10.8}$
3 – 4	$10^{-8.7}$	$10^{-9.0}$	$10^{-11.2}$
2 – 3	$10^{-10.0}$	$10^{-10.4}$	$10^{-10.0}$
1 – 2	$10^{-11.2}$	$10^{-10.0}$	$10^{-8.7}$
0 - 1	$10^{-10.8}$	$10^{-9.8}$	$10^{-9.5}$
Avg. k (m^2)	$10^{-10.0}$	$10^{-10.0}$	$10^{-10.0}$
Variance	1.0	0.5	1.0

The Q2 and Q3 rates were varied with time in the Group 4 simulations in an attempt to minimize the solute mass used by coordinating water table drawdown with the establishment of the density barrier. Figures 4.18 to 4.20 present the pumping rates used throughout the three simulations.

Figure 4.18 – Simulation p1

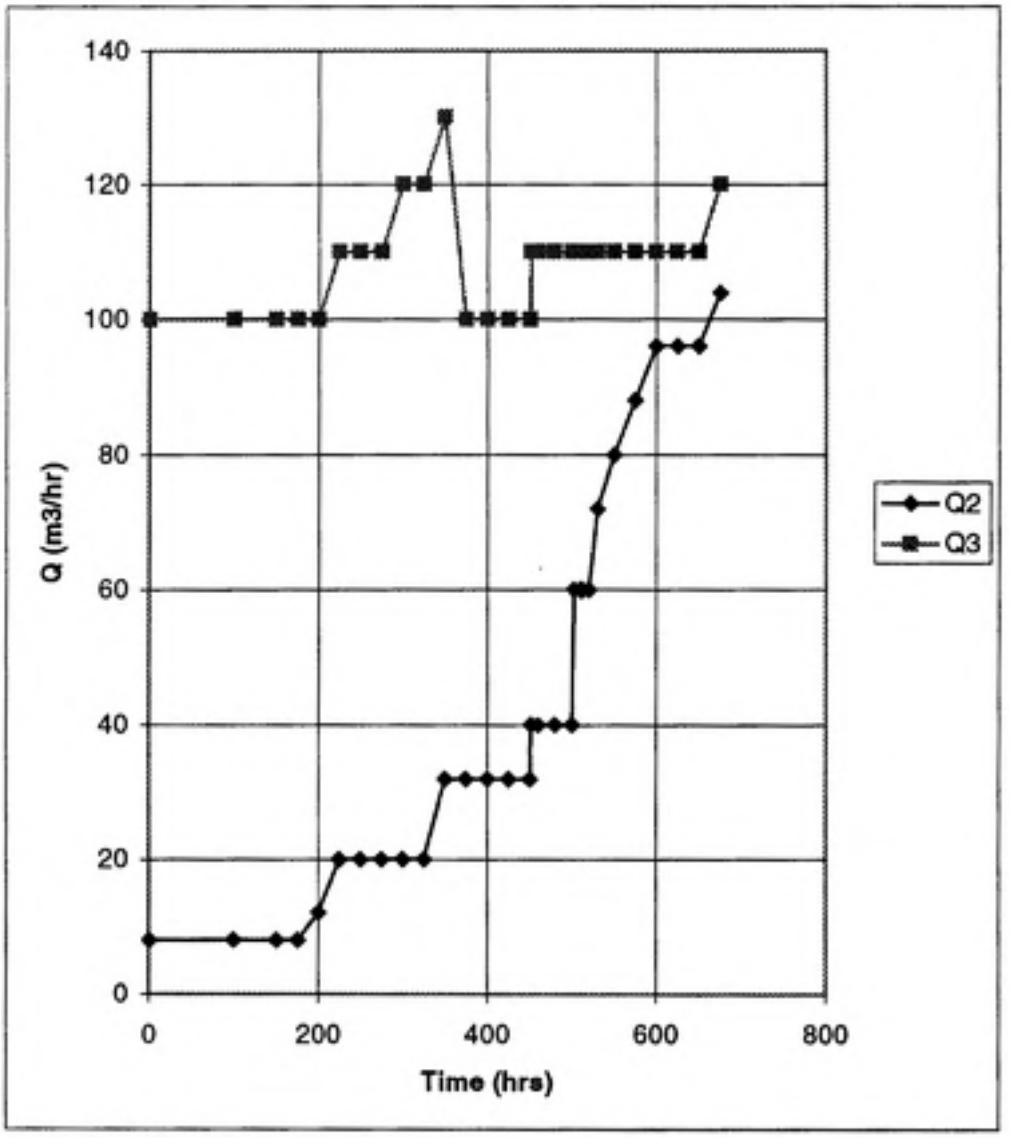

Figure 4.19 – Simulation p3

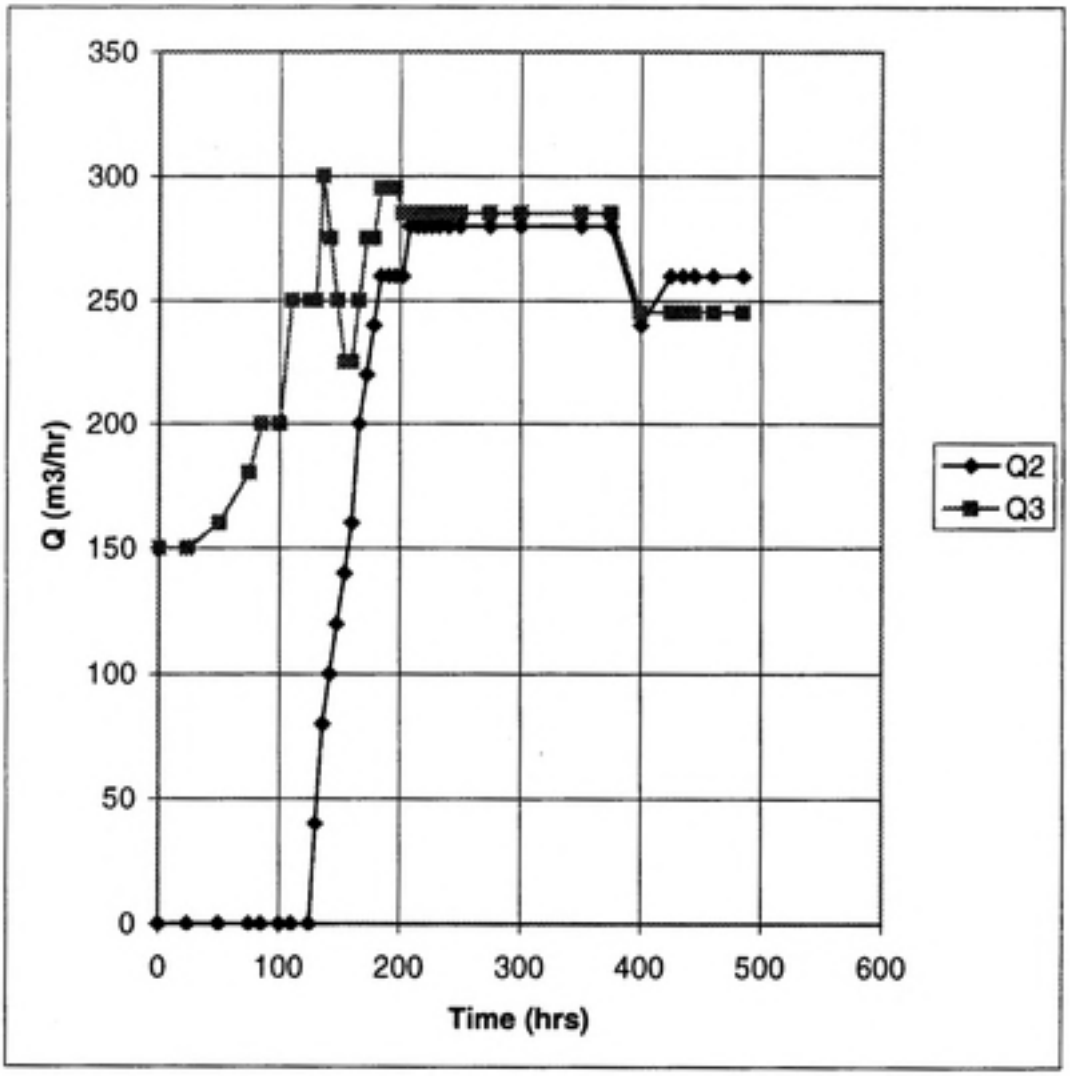

Figure 4.20 – Simulation p6

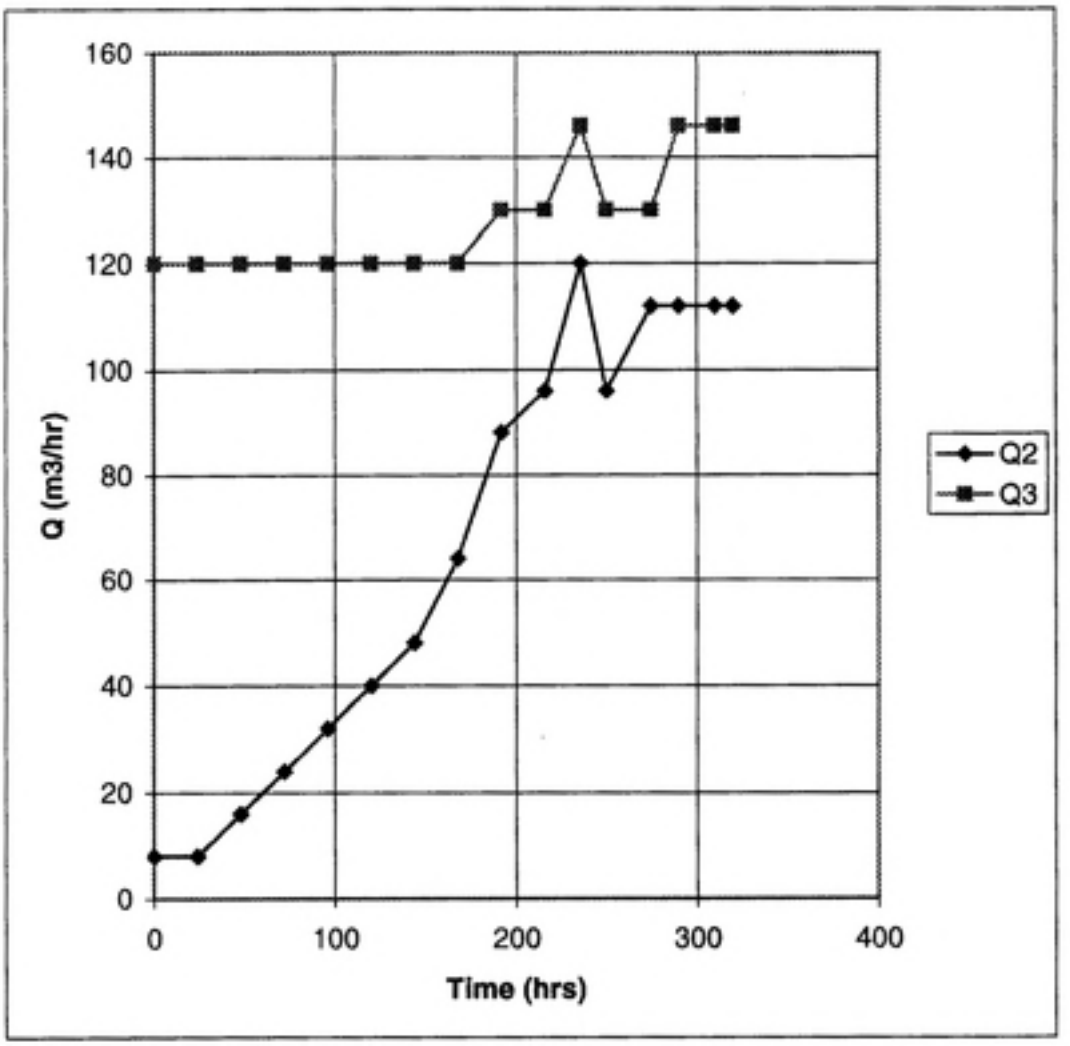

Table 4.14 summarizes the unit costs and solute mass required for the Group 4 simulations.

Table 4.14 – Group 4 Unit Cost Summary

Sim	Avg. Q2 (m3/hr)	Avg. Q3 (m3/hr)	Total Mass Injected (kg)	Mass in Barrier after Injection (kg)	Ratio Mass in Barrier to Mass Injected	Unit Cost ($M per acre)
p1	38	107	2.06E+07	5.6E+06	0.27	24.41
p3	252	269	7.19E+07	8.6E+06	0.12	50.65
p6	67	128	1.74E+07	4.7E+06	0.27	19.16

The following observations may be made with regard to the Group 4 results summarized in Table 4.14:

1. The heterogeneity represented in the Group 4 simulations significantly decreased the efficiency of solute injection compared to the homogeneous media simulations. Approximately 10 times as much solute mass was injected in the Group 4 simulations, and 73 to 88 % of the solute injected was cycled through the domain without contributing to the final density barrier volume. The solute mass remaining in the density barrier after injection is significantly higher in the Group 4 simulations than in the homogeneous media simulations, reflecting deeper density layers.

2. Of the simulations with equal variances, the simulation with lower permeabilities near the surface (p1) had a higher unit cost than the simulation with less permeable layers at the bottom of the domain

(p6). One possible explanation of this is that the low permeability layer above the mid-layer in simulation p6 limited brine spread above the middle layer, thereby promoting more horizontal spread.

3. The 1.0 variance simulations required lower pumping rates than in p3 due to the wider range in permeabilities.

4. Efficiency was lowest in the 0.5 variance simulation (p3), perhaps because of the presence of a relatively low permeability layer in the middle of the domain depth. As variance decreases, one should expect the results to approach those for a homogeneous medium. The fact that the simulation with the lowest variance resulted in the highest unit cost is reflective of the very limited set used for this comparison and illustrates that these results cannot be considered representative of conclusive trends.

4.4.5 Zero dispersivity simulation

A final simulation was performed to look at dispersivity effects. Simulation d1 is identical to simulation r1a of Group 3, except that longitudinal and transverse dispersivities are both zero in simulation d1. There is no apparent physical explanation for lack of dispersion resulting in a lower unit cost. This nonintuitive result could be attributable to numerical error in the simulation with zero dispersion. The comparison summary is presented in Table 4.16.

Table 4.16 – Summary of Simulations r1 and d1

Sim	Mass injected (kg)	Mass in density barrier after injection (kg)	Area Covered (m^2)	Avg. Q2 (m^3/hr)	Q3 (m^3/hr)	Cost per acre ($M)
r1a	5.74E+06	2.73E+06	850	80	120	5.66
d1	6.77E+06	3.05E+06	850	82	120	6.43

5 CONCLUSION

DERD is an appealing new technology for DNAPL extraction because DERD relies on mobilization of DNAPL, a more rapid mechanism for DNAPL removal than solubilization, while providing a physical barrier against uncontrolled DNAPL migration.

This report presents one conceptual model of DERD, applied to several combinations of simulated field conditions and decision variable values, in an attempt to reveal some general trends in DERD efficiency as defined by an objective function representing brine costs. The analysis presented herein is suffused with engineering judgment decisions, beginning with the number of wells and their configuration and continuing throughout each simulation with, e.g., the selection of individual and relative pumping rates and the timing of injection initialization and cessation. Consequently, this analysis does not represent a true optimization of the DERD process, but rather one individual's attempt to uncover some of the trends in process efficiency. Continued analysis of DERD will undoubtedly produce more efficient methods both in DERD process implementation and in brine recovery treatment processes.

The types of decisions made throughout this analysis, however, are the same decisions with which engineers will be faced in actual implementation of DERD. One very important and conspicuous theme in this report is that these design decisions can have a tremendous impact on the cost of DERD implementation. The cost summaries presented herein exemplify that misapplication of DERD can magnify brine costs by several factors. In practice, each DNAPL contamination site will be different, and the cost to implement DERD will rely heavily on the accuracy of measurements of site hydrogeological data and the proficiency applied to modeling and analysis of DERD to determine optimal design values. Fortunately for the design professional, there appears to be a range of optimal values for many of the decision variables through which the change

in unit cost per change in variable unit is small, providing some margin for error in design variable specification.

No attempt was made in this report to examine cost feasibility of DERD or to make comparisons of DERD costs to other technologies such as SF. Rather this report is part of the initial work to test and develop the DERD concept. Judgments regarding the cost feasibility of DERD are premature without further testing and development of the strategy, and it is perhaps justifiable to make the same statement regarding SF, which is itself a new and developing technology, particularly as applied to DNAPLs.

General DERD efficiency trends indicated by this analysis are summarized below:

- For each specific well spacing configuration, there was an optimal range of total production and total injection rates that minimized unit cost. Pumping rates below the optimal range resulted in the highest unit cost for brine. Pumping rates beyond the optimal range either failed to produce brine cost benefit (and are therefore less than optimal since pumping costs increase with pumping rate) or resulted in slightly higher brine costs.

- Brine costs were minimized by injection to production rate ratios (Q1') either near one or greater than one. Brine costs began to increase substantially with decreasing Q1' ratios at values less than 0.60.

- Brine recovery efficiency was enhanced when five wells spread out across the density barrier area were used to withdraw brine compared to brine recovery affected by the central well alone. In simulations with five wells withdrawing brine, 95 to 99% of the brine was recovered before mass fractions fell to 0.04. When the central well alone was used, approximately 90% of the brine was recovered when mass fractions fell to 0.04. Since the cost objective function was dependent solely on recovery mass fraction, increased brine recovery efficiency resulted in lower brine costs. A residual mass fraction of 0.04 translates to a high salt concentration,

40,000 mg/L, by drinking water standards, but two mitigating factors should be noted regarding this residual - 1) this concentration is localized at the production well, declining rapidly with distance from the well; and 2) simulations using multiple well brine recovery indicated that almost total recovery of the brine is possible at reasonable efficiencies.

- In homogeneous media simulations, comparison between comparable high and low permeability simulations resulted in similar brine costs and quantities, but the time required to complete the DERD process was significantly longer for the low permeability simulations, 20,000 to 42,000 hours compared to 400 to 1400 hours for high permeability simulations with the same A1 area.

- When preliminary drawdown of the watertable was not performed, DERD efficiency decreased for the high permeability simulation but not in the low permeability simulation.

- Segmentation of the simulation domain into a heterogeneous medium with varied permeability strata increased the brine cost and created difficulty in controlling the phreatic surface to maximize injection efficiency.

- In a comparison of two identical simulations with and without dispersive effects, the simulation without dispersion resulted in a higher brine cost. Since there is no apparent physical explanation for the dispersive simulation being more efficient, one might suspect numerical error in the no dispersion simulation as the cause of this curious result.

REFERENCES

(1) Bear, J., 1979, *Hydraulics of groundwater*. McGraw-Hill, New York.

(2) Bear, J., Sun Y., 1998, Optimization of pump-treat-inject (PTI) design for the remediation of a contaminated aquifer: multi-stage design with chance constraints. *Journal of Contaminant Hydrology* 29: 225-244.

(3) Chen, L. C., Knox, R. C., 1997, Using Vertical Circulation Wells for Partitioning Tracer Tests and Remediation of DNAPLs. *Ground Water Monitoring and Remediation* 14, no. 2: 161-168.

(4) Chen, Y., 1995, Using a two-dimensional sand tank to model surfactant enhanced pump-and-treat remediation of dense chlorinated hydrocarbons, Ph. D. diss., Dept. of Civil Engineering and Environmental Sciences, University of Oklahoma, Norman.

(5) Chevalier, L. R., Masten, S. J., Wallace, R. B., Wiggert, D. C., 1997, Experimental Investigation of Surfactant-Enhanced Dissolution of Residual NAPL in Saturated Soil. *Ground Water Monitoring and Remediation* 14, no. 2: 89-98.

(6) Culver, Teresa B. and Shoemaker, Christine A., 1993, Optimal control for groundwater remediation by differential dynamic programming with quasi-newton approximations. *Water Resources Research* 29, no. 4: 823-831.

(7) Domenico, P. A. and Schwartz, F. W., *Physical and Chemical Hydrogeology*. John Wiley and Sons, New York, 1990.

(8) Forsyth, P. A. and Sudicky, E. A., 1997, Discrete well bore simulations of pump-and-treat strategies for remediation of LNAPL contaminated aquifers. *Journal of Contaminant Hydrology* 31: 57-81.

(9) Gordon, Matthew J., 1998, Case history of a large-scale air sparging/soil vapor extraction system for remediation of chlorinated volatile organic compounds in ground water. *Ground Water Monitoring and Remediation* 11, no. 2: 137-149.

(10) Haley, Jennifer L., Hanson, Bill, Enfield, Carl, and Glass, John, 1991, Evaluating the effectiveness of groundwater extraction systems. *Ground Water Monitoring and Remediation* 11, no. 1: 119-124.

(11) Ho, W. S., and Kamalesh K. Sirkar, *Membrane Handbook*. Chapman & Hall, New York, 1992.

(12) Huntress, Ernest Hamlin, *The Peparation, Properties, Chemical Behavior, and Identification of Organic Chlorine Compounds.* John Wiley & Sons, New York, 1948.

(13) Ibaraki, Motomu, 1997, A robust and efficient numerical model for analyses of density-dependent flow in porous media. *Journal of Contaminant Hydrology* 34: 235-246.

(14) Kipp, Kenneth L., HST3D: A computer code for simulation of heat and solute transport in three-dimensional ground-water flow systems. Water-Resources Investigations Report 86-4095.

(15) Lipe, K. Michelle, Sabatini, David A., Hasegawa, Mark A., and Harwell, Jeffrey H., 1996, Micellar-enhanced ultrafiltration and air-stripping for surfactant-contaminant separation and surfactant reuse. *Ground Water Monitoring and Remediation* : 85-92.

(16) Lobo, V. M. M. and Quaresma, J. L., *Handbook of Electrolyte Solutions, Part B,* Elsevier Science Publishing Company, Inc., New York, 1955.

(17) Martel, R., Gelinas, P. J., Saumure, L., 1998, Aquifer washing by micellar solutions: 3 Field test at the Thouin Sand Pit. *Journal of Contaminant Hydrology* 30: 33-48.

(18) Michalski, Andrew , Metlitz, Michael N., and Whitman, Ira L., 1995, A field study of enhanced recovery of DNAPL pooled below the water table. *Ground Water Monitoring and Remediation* : 90-100.

(19) Miller, C. T., Hill, E. H., and Moutier, M., 1999, Remediation of DNAPL-contaminated subsurface systems using density-motivated mobilization. *Environmental Science and Technology* .

(20) Miller, C. T., 1999, Density-enhanced remediation of dense non-aqueous phase liquid contamination of subsurface environments.

(21) Oolman, T., Godard, S. T., Pope, G. A., Jin, M., and Kirchner, K., 1995, DNAPL flow behavior in a contaminated aquifer: evaluation of field data. *Ground Water Monitoring and Remediation* : vol. 15, no. 4: 125-137.

(22) Pontius, Frederick W., *American Water Works Association: Water Quality and Treatment*. McGraw-Hill, Inc., 1990.

(23) Powers, Susan E., Nambi, Indumanthi M., and Curry, Garrey W., 1998, Non-aqueous phase liquid dissolution in heterogeneous systems: Mechanisms and a local equilibrium modeling approach. *Water Resources Research* 34, no. 12: 3293-3302.

(24) Rothmel, Randi K., Peters, Robert W., St. Martin, Edward, and Deflaun, Mary F., 1998, Surfactant Foam/bioaugmentation technology for in situ treatment of TCE-DNAPLs. *Environmental Science and Technology* 32, no. 11: 1667-1675.

(25) Sabatini, David A., Knox, Robert C., Harwell, Jeffrey H., and Wu, Bin, 1999, Integrated design of surfactant enhanced NAPL remediation: overview and surfactant selection for Dover AFB demonstration test. *Journal of Contaminant Hydrology*

(26) Saladin, Paolo and Fiorotto, Virgilio, 1998, Solute transport in highly heterogeneous aquifers. *Water Resources Research* 34, no. 5: 949-961.

(27) Shook, G. Michael, Pope, Gary A., Kostarelos, K., Prediction and minimization of vertical migration of DNAPLs using surfactant enhanced aquifer remediation at neutral buoyancy. *Journal of Contaminant Hydrology* 34: 363-382.

(28) Zaytsev, I. D. and Aseyev, G. G., *Properties of aqueous solutions of electrolytes,* CRC Press, Inc, Boca Raton, Fla., 1992.

(29) Zhang, Hubao, Schwartz, Frank W., Wood, Warren W., Garabedian, S. P., LeBlanc, D. R., 1998, Simulation of variable-density flow and transport of reactive and noreactive solutes during a tracer test at Cape Cod, Massuchusetts. *Water Resources Research* 34, no. 1: 67-82.